An Introduction to Operational Modal Identification of Offshore Wind Turbine Structures

Damgaard, Mads

Publication date:
2011

Document Version
Publisher's PDF, also known as Version of record

An Introduction to Operational Modal Identification of Offshore Wind Turbine Structures

Mads Damgaard

ISSN 1901-7286
DCE Technical Memorandum No. 13

AALBORG UNIVERSITY
Department of Civil Engineering

Aalborg University
Department of Civil Engineering
Water and Soil

DCE Technical Memorandum No. 13

An Introduction to Operational Modal Identification of Offshore Wind Turbine Structures

by

Mads Damgaard

December 2011

Scientific Publications at the Department of Civil Engineering

Technical Reports are published for timely dissemination of research results and scientific work carried out at the Department of Civil Engineering (DCE) at Aalborg University. This medium allows publication of more detailed explanations and results than typically allowed in scientific journals.

Technical Memoranda are produced to enable the preliminary dissemination of scientific work by the personnel of the DCE where such release is deemed to be appropriate. Documents of this kind may be incomplete or temporary versions of papers—or part of continuing work. This should be kept in mind when references are given to publications of this kind.

Contract Reports are produced to report scientific work carried out under contract. Publications of this kind contain confidential matter and are reserved for the sponsors and the DCE. Therefore, Contract Reports are generally not available for public circulation.

Lecture Notes contain material produced by the lecturers at the DCE for educational purposes. This may be scientific notes, lecture books, example problems or manuals for laboratory work, or computer programs developed at the DCE.

Theses are monograms or collections of papers published to report the scientific work carried out at the DCE to obtain a degree as either PhD or Doctor of Technology. The thesis is publicly available after the defence of the degree.

Latest News is published to enable rapid communication of information about scientific work carried out at the DCE. This includes the status of research projects, developments in the laboratories, information about collaborative work and recent research results.

Published 2011 by
Aalborg University
Department of Civil Engineering
Sohngaardsholmsvej 57,
DK-9000 Aalborg, Denmark

Printed in Denmark at Aalborg University

ISSN 1901-7286 DCE Technical Memorandum No. 13

Preface

The present technical memorandum “An Introduction to Operational Modal Identification of Offshore Wind Turbine Structures” is prepared in connection with an ongoing Ph.D study at Aalborg University. The memorandum is intended for use in the civil engineering field and may serve as an inspiration to experimental modal analysis of complex dynamically loaded structures.

A huge number of papers have been published in the last years within traditional experimental modal analysis. However, for large civil engineering structures accurate model identification under actual operating conditions is difficult to extract by traditional experimental technologies. Operational modal analysis allows extracting modal parameters based on measuring only the response of a structure and using the ambient or natural operating forces as unmeasured input. Originally, operational modal analysis was developed for modal estimation of civil engineering structures like buildings, towers and bridges. Today, the technology is used for mechanical structures like ships, aircraft, vehicles and wind turbines. However, the loading forces for mechanical structures are complex. For a wind turbine structure a combination of harmonic excitation originating from the rotating rotor and broadband excitation from air turbulence is present, which sets limitations on the applicability of operational modal analysis to wind turbine structures.

The technical memorandum contains an introduction to the theory within experimental modal analysis and, in particular, to operational modal identification. Examples of structural assessment of wind turbines by operational identification are included.

Aalborg, December 2011 Mads Damgaard

Contents

CHAPTER 1
Introduction

In order to meet the European Union's commitment to reduce the consumption of fossil fuels, wind energy is proving its potential as an important part of the solution. Especially offshore wind energy has potential to be a competitive energy source due to high wind intensity with low turbulence. However, correlation between water depth and cost of energy is observed for offshore wind turbine structures. Significant research and development are needed in order to avoid an increase in the cost per MW power when the turbines are installed at greater water depths. Hence, the dynamic properties of the wind turbine structures are crucial in order to obtain a cost effective design. In this introduction a brief overview of offshore wind turbine structures and their characteristics are given. Further, the main objectives of the technical memorandum are presented.

1.1 Background

Within the last 30 years the need of alternative energy sources has been given great attention. During the period wind turbines have grown from producing less than 100 kW to more than 6 MW. Wind energy is currently the fastest-growing energy source in the world. According to Global Wind Energy Council (2010) the total installed capacity of wind power has grown at an average rate of 59% per year over the years 2002-2010, see Fig. 1–1a. The growth of wind power in the last years has mainly been driven by China which is now the country with the largest installed wind power capacity in the world. China has slipped past the USA to become the world's leading wind power country. Despite a level of uncertainty in prognositication, the Global Wind Energy Council (2010) forecasts every year the global wind market developments for the coming five years. Asia, North America and Europe will contribute to drive the expansion of wind energy capacity, where Asia will remain the faster growing market in the world driven primarly by China, see Fig. 1–1b.

At this writing the majority of wind turbines are located onshore due to lower construction costs. However, the population density and existing buildings restrict suitable wind turbine locations on land, which justifies the development of offshore wind energy. Contrary to onshore wind turbines, the size of offshore wind turbines is not limited by logistic problems during transportation of large structural components. The amazing growth in the installed capacity of onshore and offshore wind turbines, however, requires many challenges within civil engineering and science to be solved. Overall, the price of offshore wind energy must decrease in order to be competitive with present alternatives. As a consequence wind turbines are increased significantly in size with larger rotors and more powerful generators. The costs are kept as low as possible by reducing the overall weight, which leads to very slender and flexible structures. Thus, the eigenfrequencies are typically below 0.3 Hz. An improper design may cause resonance due to the excitation from

wind and waves, leading to immature failure in the fatigue limit state (FLS). This in turn necessitates a correct estimate of the basic dynamic properties of the entire wind turbine structure, such as natural frequencies and damping properties, as these are essential for the dynamic behaviour.

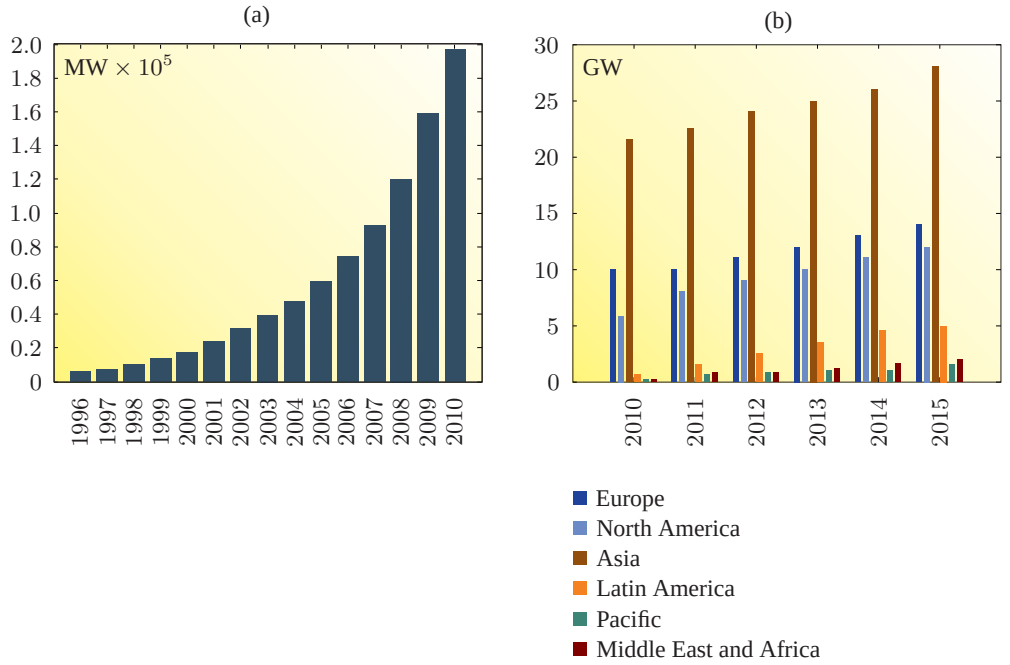

Figure 1–1 Wind power market around the world: (a) Global cumulative installed wind capacity 1996-2010, (b) Cumulative market forecast by region 2010-2015. After Global Wind Energy Council (2010).

1.2 Excitation Range of Offshore Wind Turbines

According to API (2000) and DNV (2001) four limit states have to be considered for designing offshore wind turbines. Firstly, the maximum load carrying resistance of the structure must be defined by the ultimate limit state (ULS). Secondly, the stiffness of the structure should ensure that the displacements and rotations in seabed correspond to a tolerance criterion applicable to normal use by consider the serviceability limit state (SLS). Thirdly, failure due to the effect of cyclic loading must be analysed in the fatigue limit state (FLS). Finally, the maximum load-carrying capacity for rare accidental loads must be found in the accidental limit state (ASL). However, besides these design analyses a detailed knowledge of the expected frequencies of the excitation forces and the natural frequencies of the wind turbine is crucial. Without sufficient damping, the resonant behaviour of the turbine can cause severe load cases which especially induce fatigue. Modern offshore wind turbines have a rotational speed typically in the range 10-20 revolutions per minute which means that the first excitation frequency 1P is in the range 0.17-0.33 Hz. The second excitation frequency is the blade passing frequency N_bP, where N_b is the number of blades. For a three-bladed wind turbine the blade passing frequency is in the range 0.5-1.0 Hz. For the North Sea, the wave spectrum for engineering purposes is often described

by the Joint European North Sea Wave Project (JONSWAP) spectrum with a typical frequency range of wave energy between 0.05 Hz to 0.14 Hz (Liu and Frigaard 2001).

By using the Kaimal spectrum to represent the wind power spectrum according to DNV (2010) it is possible to illustrate the excitation range 1P and 3P and the realistic spectra representing aerodynamic and hydrodynamic excitation in Fig. 1–2. To avoid resonance, the offshore wind turbine should be designed such that its first natural frequency f_1 does not coincide with either 1P and 3P. Hence, three possible designs can be chosen. A very stiff structure with the first natural frequency f_1 above 3P ("stiff-stiff"), first natural frequency f_1 in the range between 1P and 3P ("soft-stiff") or a very soft structure with the first natural frequency f_1 below 1P ("soft-soft"). A "soft-stiff" wind turbine structure is often chosen in current practice due to a huge amount of steel is required for a "stiff-stiff" structure. As the trend is to create larger turbines, the rotor blades become longer, generator masses greater and the hub height higher. Thus, the rotation frequency and the first natural frequency will decrease. It may then seem impossible to design wind turbine structures as a "soft-soft" structure, since the risk of the hydrodynamic frequency range falls into 1P is relatively high.

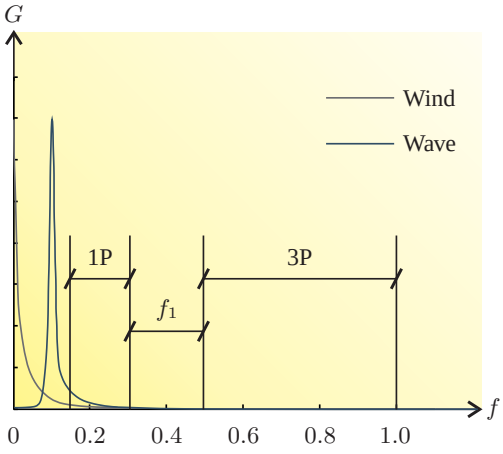

Figure 1–2: Excitation range for a modern offshore wind turbine structure. After Leblanc (2009).

1.3 Wind Turbine Dynamics

Wind energy is a fast-growing interdisciplinary field that involves many different disciplines within civil engineering and science. The behaviour of wind turbine structures is made up of a complex interaction of components and subsystems. The main components consist of the tower, foundation, nacelle and rotor as shown in Fig. 1–3. The rotor blades rotate around the horizontal hub and capture the kinetic energy in the wind and transform it into the rotational kinetic energy of the wind turbine. The hub is usually connected to a gearbox and a generator which is located inside the nacelle. It should be mentioned that direct-drive generators are present as well and makes the gearbox unnecessary. Wind turbines may be variable pitch or fixed pitch meaning that the blades may or may not be able to rotate along their longitudinal axes. Moreover, wind turbines have a yaw mechanism, which is used to turn the wind turbine rotor against the wind.

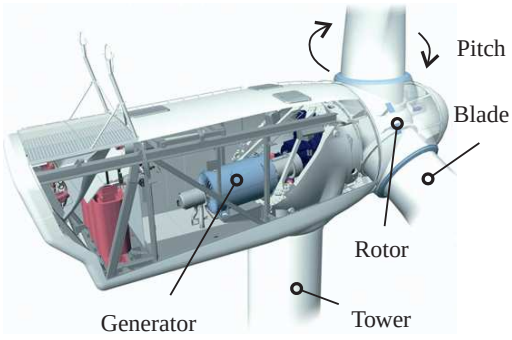

Figure 1–3: Key components of a Vestas V90 2 MW. After Vestas (2011).

Obviously, the wind causes the rotor to turn. However, it is a bit more complicated than just the air molecules hitting the front of the rotor blades. Wind turbine blades are shaped as airfoils to make the air flow faster on one side and slower on the other. This means that the pressure will be lowest on the curved side which creates a lift force F_{L} perpendicular to the wind direction and a drag force F_{D} parallel to the wind direction. The principle of a lifting surface for a wind turbine wing is illustrated in Fig. 1–4. The rotation is assumed from right to left, which induced a horizontal wind component F_{M}. Hence, an angle θ between the resultant wind component F_{R} and the incoming wind component F_{wind} appears. The wind flow generates a pressure and a suction on the different sides of the surface, which initiates the lift force F_{L} and the drag force F_{D}. The two forces can be projected onto the tangential and normal direction. As long as the tangential force F_{T} is in the rotational direction, a positive torque is produced on the spinning axis for generating electricity. The normal force F_{N} and the tangential force F_{T} cause bending deformation in the flapwise direction and edgewise direction, respectively. The reader is referred to the Danish Wind Industry Association (2011) for further reading about wind turbine technology.

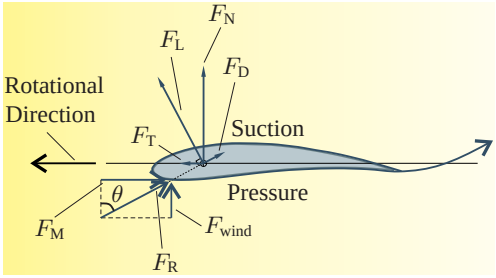

Figure 1–4: Aerodynamic principle for a wind turbine blade. After Larsen (2005).

A lot of experience in designing offshore support structures within oil and gas exist. However, these structures are dominated by a huge self weight which reduces the exposure to dynamic excitation. The loading of offshore wind turbines is quite different. Strong cyclic loading originating from rotor blades, wind and waves excite the structure. Offshore support structures within oil and gas, high-rise buildings and large cablestayed bridges are all characterised by the fact, that the mass distribution is constant during time. The presence of rotor blades passing the flexible tower in a high altitude cause a time dependent mass distribution for wind turbine structures. In addition, wind turbines are, under the right circumstances, affected by gyroscopic forces due to the rotating rotor. In principle, two motions of the wind turbine will cause the gyroscopic forces. In the case where the rotating rotor is yawed into the wind, a torque perpendicular to the spinning axis and yawing axis will arise, see Fig. 1–5a. However, an active yaw control system will ensure a slow yawing rate, which makes the gyroscopic forces insignificant. Gyroscopic effects can also occur, when the wind turbine is exposed to a bending moment perpendicular to the spinning axis and yawing axis, which cause the rotating rotor to tilt upwards and downwards. As a consequence, a torque is introduced around the tower axis, see Fig. 1–5b. (Jensen 2011)

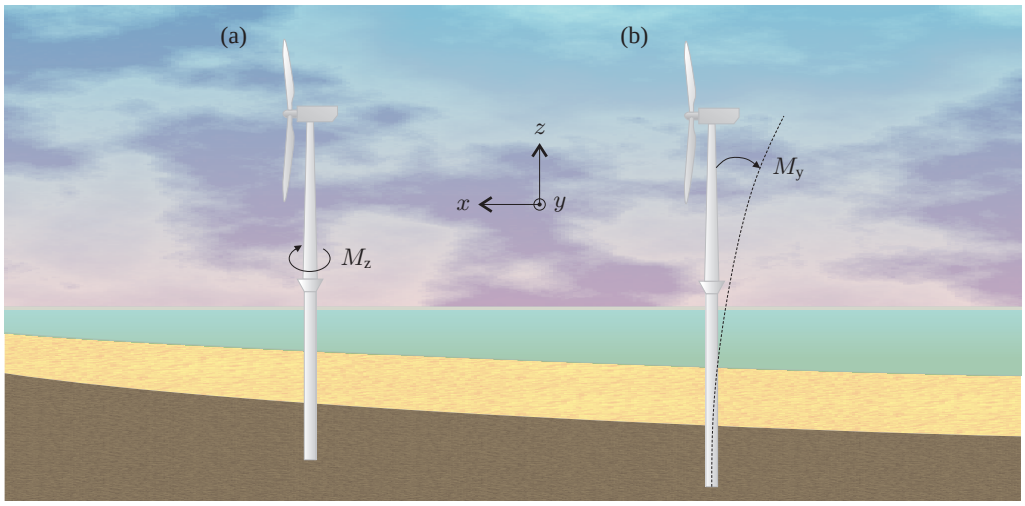

Figure 1–5 Gyroscopic effects for wind turbine structures: (a) The rotating rotor is yawed into the wind. Hence, the yaw moment M_z causes an additional bending moment around the y-axis, (b) The rotating rotor tilts upwards and downwards due to a cyclic moment M_y. This introduces a torsional moment around the z-axis.

1.4 Overall Aim and Specific Objectives

As earlier outlined wind energy is expected to be a dominating energy source in the coming years. The increasing size of the wind turbines and the demand for cost efficient turbines mean, that the turbine system becomes more flexible and thus more dynamically active. This calls for an accurate numerical model that identifies the dynamic properties of the wind turbine structure. However, such a model is characterised by limitations and assumptions that may be difficult to justify without experimental tests. Despite of the complex dynamic behaviour of wind turbines as described in Section 1.3, a numerical linear modal analysis is widely used in civil engineering practice. The method allows the complex multi-degree-of-freedom (MDOF) system to be broken into several independent single-degree-of-freedom (SDOF) systems, each accounting for the behaviour of a given mode of the offshore wind turbine structure. For modal analysis of an offshore wind turbine supported by a monopile foundation, it is common to model the tower and foundation as elastic beams. The foundation is supported by linear soil springs and the concentrated nacelle mass is placed at the top node with actual eccentricity and mass inertial moments. The transition piece is represented by a beam element with equivalent stiffness and mass properties, and weights of appurtenances are included as lumped masses. To what extent this calculation procedure is sufficient to obtain correct estimates of the dynamic properties of an offshore wind turbine structure can be validated by experimental modal analysis.

The overall aim and specific objectives in this technical memorandum are within experimental modal analysis. Traditional experimental modal analysis or input-output modal identification, is a well-known technique to determine the natural frequencies, damping ratios and mode shapes of structures. However, this technique requires that the input force and the output response are known. For large civil engineering structures the input excitation is difficult to measure and the modal properties are almost impossible to estimate. Operational modal identification, also denoted as ambient modal analysis or output only modal identification, is a complementary

technique to the traditional modal analysis technique and is based upon measuring only the responses of test structures. An important feature of using operational modal analysis is that the dynamic properties of the structure are determined within true boundary conditions and actual force and vibration levels. The method has been used for different civil engineering structures. However, while civil engineering structures are mainly loaded by ambient stochastic forces like wind, waves and traffic loads, the loading forces of a wind turbine are much more complicated. Time-invariance of the structure during the test is a general requirement in modal testing, *i.e.* the structure under test remains the same during the test. This is not the case for a operational wind turbine structure. The nacelle revolves about the tower, the rotor rotates about its axis and the blades pitch depending of the wind speed and rotor speed. This in turn gives raise to the following objectives for the technical memorandum:

1. An introduction to the basic theory within experimental modal analysis. This includes a clarification of pertinent concepts and fundamental definitions related to the dynamic behaviour of physical structures. The reader is introduced to general descriptions and properties of random data and digital signal processing.

2. A description of the difference between traditional experimental modal analysis techniques and operational modal identification techniques. This calls for an introduction to the theory within operational modal identification, where assumptions and limitations are discussed.

3. An explanation of the validity of operational modal identification within offshore wind energy. The dynamic behaviour of offshore wind turbine structures differ from other civil engineering structures. A literature review of operational modal identification is conducted with the purpose of clarifying to what extent operational modal identification has been used within offshore wind energy.

CHAPTER 2
The Basics of Experimental Modal Analysis

In this chapter, the basic theory of experimental modal analysis is described. Firstly, the application of system identification is explained with focus on modal analysis. Secondly, the chapter includes a description of the fundamental theory of stationary random processes and structural dynamics. The derivation and description of these theories form the theoretical basis of experimental modal analysis. Finally, general digital data analysis is explained that are required prior to the main estimation of the structural modal parameters.

2.1 Introduction

Vibration measurements of civil engineering structures have been practiced for many years. However, in the recent years the number of dynamic tests has increased tremendously. The design and construction of more and more complex and ambitious civil structures requires accurate identification of the structural dynamic properties. Thus, experimental analysis provides reliable data to support calibrating, updating and validating of numerical models used in the design phase. Civil structures like high-rise buildings, dams, large cablestayed or suspension bridges all show highly dynamic behaviour in their service life. However, determination of the dynamic behaviour of offshore wind turbine structures may be even more difficult than these structures. Besides cyclic wind and wave loads, wind turbine structures are exposed to periodic loading from the rotor blades and in case of emergency stops or too high wind velocity the rotor blades pitch out of the wind. The rotor blades thus have to be able to turn around their longitudinal axis. During the last years, wind turbines have increased tremendously in both size and performance. In order to stay competitive, the overall weight of the foundation and turbine must be kept on a minimum, which results in a flexible structure. Thus, the eigenfrequencies of the structure are close to the excitation frequencies related to environmental loads from wind and waves. The highly variable and cyclic loads on rotor, tower and foundation all demand special fatigue design considerations and create an even greater demand for a fuller appreciation of how the turbine ages structurally over its service life.

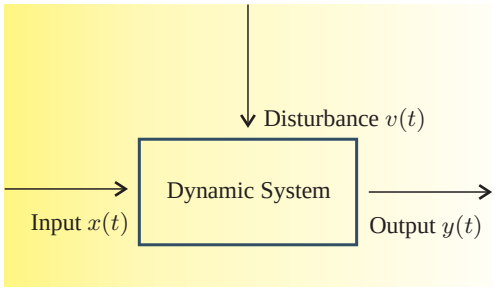

Figure 2–1: Dynamic system with input x(t) and output y(t). After Andersen (1997).

In order to describe a dynamic system, mathematical models represented in either the time or frequency domain are useful. Overall, the mathematical models can either be constructed by physical modelling or by system identification. For the physical modelling the representation of the dynamic system is based on pure physics and fundamental laws, such as Newton equations. However, in case of limit physical knowledge about the dynamic system, it can be difficult or almost impossible to establish qualified mathematical models and for that reason system identification is beneficial. By use of statistical methods, system identification is able to establish mathematical models of a dynamic system calibrated from measured data. A mixture of the two methods is possible, *i.e.* some parts of the system identification model can have physical origin (Andersen 1997). In Fig. 2–1 an illustration of a linear dynamic system can be seen. The dynamic system is subjected to a well-defined single input $x(t)$ from a stationary random process $\{x(t)\}$ and produces a well-defined output $y(t)$. Furthermore, the system is affected by some disturbance $v(t)$. The output $y(t)$ will belong to a stationary random process $\{y(t)\}$ and describes how the system responds to the applied input. For that reason the output will be a mixture of dynamic response of the system and characteristic of the input and disturbance. In closely-controlled conditions it is possible to measure both the input, the disturbance and the output, whereas the input and disturbance of large civil engineering structures are not easily measured and thereby often unknown.

2.1.1 Modal Analysis

For civil engineering structures system identification is often used in order to perform a modal analysis and estimating modal parameters that describe specific dynamic characteristics of the structure. In general, modal analysis can be characterised in the following way:

The process involved in testing components or structures with the objective of obtaining a mathematical description of their dynamic or vibration behaviour

How comprehensive the mathematical model is, depends on the application. It can be an estimate of natural frequencies and damping ratios in one case and a full mass-spring-dashpot model for the next. The following modal parameters can be considered from a modal analysis:

- Modal Frequency
- Modal Damping
- Modal Vectors

The modal frequency is often referred to as the resonance frequency or eigenfrequency. Modal damping is characterised by the damping ratio that indicates the degree to which the structure itself is able of damping out vibrations. Finally, the modal vectors are the mode shapes, *i.e.* the way the structure moves at a certain resonance frequency.

Experimental modal analysis has been used widely in civil engineering for the last decades. In the classical modal theory, input-output modal identification, the modal parameters are found

by fitting a model to the so-called frequency response function, a function relating excitation and response. However, input-output modal identification requires that the input loading and the output response is measured. As mentioned earlier the loading of large civil engineering structures is not easily measured under operational conditions and it is difficult to excite them artificially. For that reason the modal identification must be based on the measured response only. In this method the modal parameters are estimated by simple peak picking. Further description of the theory and the applicability of operational modal identification are presented in Chapter 3.

In the following two sections the fundamental theory related to stationary random processes and structural dynamics is presented. The two sections will form a foundation for applications of experimental modal analysis.

2.2 Stationary Random Process

Data analysis used for engineering practice often deals with determination of the dependency of two or more sets of data. The relationships are generally found by a correlation function or its Fourier transform, the so-called spectral density function. The section is based on Bendat and Piersol (1980, 2000) and Ewins (2000).

2.2.1 Correlation Functions

Data representing a physical phenomenon do often consist of several single time histories $x_{\mathrm{k}}(t)$. Each single time history is called a sample function or a sample record and will often be unique. For that reason the data are considered random. The collection of all possible sample functions, that the random phenomenon might have produced, is called a random process or a stochastic process $\{x(t)\}$. If the random process $\{x(t)\}$ consists of n sample records the mean value of the random process can be computed at any specific time t_1

$$\mu_x(t_1) = \lim_{n\to\infty} \frac{1}{n} \sum_{k=1}^{n} x_{\mathrm{k}}(t_1) \tag{2–1}$$

In a similar manner a correlation between the values of the random process at two different times t_1 and $t_1 + \tau$, denoted as the autocorrelation function $R_{\mathrm{xx}}(t_1, t_1 + \tau)$, can be found

$$R_{\mathrm{xx}}(t_1, t_1 + \tau) = \lim_{n\to\infty} \frac{1}{n} \sum_{k=1}^{n} x_{\mathrm{k}}(t_1) x_{\mathrm{k}}(t_1 + \tau) \tag{2–2}$$

In case of $\mu_x(t_1)$ and $R_{\mathrm{xx}}(t_1, t_1 + \tau)$ vary as time t_1 varies the random process $x_{\mathrm{k}}(t)$ is said to be nonstationary. For the special case where $\mu_x(t_1)$ and $R_{\mathrm{xx}}(t_1, t_1 + \tau)$ remain constant with changes in the time t_1, the data is said to be stationary. For stationary data the average value $\mu_x(t_1)$ and the autocorrelation $R_{\mathrm{xx}}(t_1, t_1 + \tau)$ will equal the corresponding average and autocorrelation value computed over time from a single sample record. This results in the following expressions

$$\mu_x(k) = \lim_{n\to\infty} \frac{1}{T} \int_0^T x_{\mathrm{k}}(t)dt \tag{2–3}$$

$$R_{xx}(\tau,k) = \lim_{T\to\infty}\frac{1}{T}\int_0^T x_k(t)x_k(t+\tau)dt \tag{2–4}$$

The autocorrelation function $R_{xx}(\tau,k)$ for a stationary record is a measure of time-related properties in the data that are separated by fixed time delays. In other words, it contains information about how quickly random processes or random records change with respect to time. From its definition, the autocorrelation function is always an even function of τ, which means $R_{xx}(-\tau,k) = R_{xx}(\tau,k)$. Fig. 2–2 illustrates the autocorrelation for wide bandwidth random noise. It should be noted that the autocorrelation for $\tau = 0$ is the mean square value of the data ψ_x^2. Moreover, the autocorrelation collapses to a constant value equal to the square of the mean μ_x^2 as τ increases. In case of more than one random signal is being applied to a system, it is important to describe the relationship between the random processes. Consider two random processes $\{x(t)\}$ and $\{y(t)\}$ which are assumed to be stationary. Hence, they can be represented by individual time history records $x_k(t)$ and $y_k(t)$. By introducing a time delay τ between $x_k(t)$ and $y_k(t)$, the so-called cross-correlation function is given by

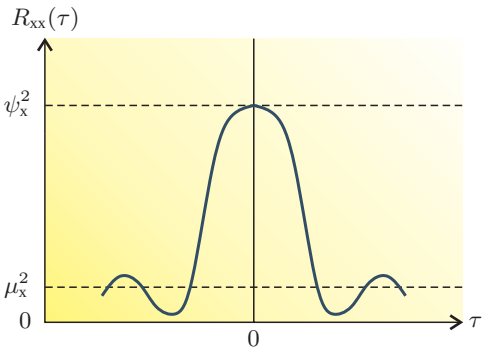

Figure 2–2: The autocorrelation function for wide bandwidth random noise. After Bendat and Piersol (1980).

$$R_{xy}(\tau,k) = \lim_{T\to\infty}\frac{1}{T}\int_0^T x_k(t)y_k(t+\tau)dt \tag{2–5}$$

The discrete time formulation for estimating the cross-correlation function can be written as follow

$$R_{xy}(t_1,t_1+\tau) = \lim_{n\to\infty}\frac{1}{n}\sum_{k=1}^{n} x_k(t_1)y_k(t_1+\tau) \tag{2–6}$$

2.2.2 Spectral Density Functions

As earlier mentioned the spectral density function can be found by Fourier transform of a correlation function. More specific, the cross-spectral density function between two time history records $x_k(t)$ and $y_k(t)$ representing the stationary random processes $\{x(t)\}$ and $\{y(t)\}$ is determined by the Fourier transform of the cross-correlation function between those records

$$S_{xy}(f,k) = \int_{-\infty}^{\infty} R_{xy}(\tau,k)e^{-i2\pi f\tau}, \tag{2–7}$$

where i is the imaginary unit and f is the frequency. For the special case where $y_k(t) = x_k(t)$ the autospectral density function, also denoted the power spectral density function, becomes

$$S_{xx}(f,k) = \int_{-\infty}^{\infty} R_{xx}(\tau,k)e^{-i2\pi f\tau} \tag{2–8}$$

Eq. (2–7) and Eq. (2–8) define the spectral density functions for all frequencies and are often denoted as two-sided spectra. From the symmetry properties of the stationary autocorrelation function, the following expressions yield for the auto spectral density function

$$S_{\mathrm{xx}}(-f,k) = S^*_{\mathrm{xx}}(f,k) = S_{\mathrm{xx}}(f,k), \tag{2–9}$$

where superscript * denotes complex conjugate. Another way of defining the spectral density functions is by use of Fourier transforms on the original data records. By considering a pair of sample records $x_{\mathrm{k}}(t)$ and $y_{\mathrm{k}}(t)$ from two stationary random processes $\{x(t)\}$ and $\{y(t)\}$, the spectral density functions can be defined for a finite time interval $0 \leq t \leq T$ as

$$S_{\mathrm{xx}}(f,T,k) = \frac{1}{T} X^*_{\mathrm{k}}(f,T) X_{\mathrm{k}}(f,T) \tag{2–10a}$$

$$S_{\mathrm{xy}}(f,T,k) = \frac{1}{T} X^*_{\mathrm{k}}(f,T) Y_{\mathrm{k}}(f,T), \tag{2–10b}$$

where $X_{\mathrm{k}}(f,T)$ and $Y_{\mathrm{k}}(f,T)$ represent finite Fourier transforms of $x_{\mathrm{k}}(t)$ and $y_{\mathrm{k}}(t)$

$$X_{\mathrm{k}}(f,T) = \int_0^T x_{\mathrm{k}}(t) \mathrm{e}^{-i2\pi ft} dt \tag{2–11a}$$

$$Y_{\mathrm{k}}(f,T) = \int_0^T y_{\mathrm{k}}(t) \mathrm{e}^{-i2\pi ft} dt \tag{2–11b}$$

For T tending toward infinity, the estimates of $S_{\mathrm{xx}}(f)$ and $S_{\mathrm{xy}}(f)$ is given by

$$S(f) = \lim_{T\to\infty} \mathrm{E}\left[S_{\mathrm{xx}}(f,T,k)\right] \tag{2–12a}$$

$$S(f) = \lim_{T\to\infty} \mathrm{E}\left[S_{\mathrm{xy}}(f,T,k)\right] \tag{2–12b}$$

In practice it is more convenient to work with spectra defined over positive frequencies only. These are called one-sided spectral density functions and are defined as

$$G_{\mathrm{xx}}(f) = 2S_{\mathrm{xx}}(f) \tag{2–13a}$$

$$G_{\mathrm{xy}}(f) = 2S_{\mathrm{xy}}(f) \tag{2–13b}$$

2.3 Basic Theory of Linear Structural Dynamics

In spite of the fact that practical structures can not be modelled as a single degree of freedom (SDOF) system, the theory is important, as a complex multi degree of freedom (MDOF) system often can be represented as a linear superposition of a number of SDOF characteristics. Thus, a thorough description of SDOF systems will be introduced in this section, just like the theory of MDOF systems will take place. It should be noted that linearity of the dynamic systems is assumed, which is often not the case for real systems. For example, a loading-strain relationship for concrete will actually start deviating from a linear relationship long before material failure. However, the response characteristic may be assumed linear for many physical systems, at least over some limited range of inputs without involving great errors. The section is based on Damkilde (1998), Bendat and Piersol (2000), Ewins (2000) and Nielsen (2004).

2.3.1 Single Degree of Freedom System Theory

In Fig. 2–3 a SDOF system is shown. The system consists of a point mass m, a massless linear elastic spring with the spring constant k and a viscous damper characterised by the constant c, that transforms kinetic energy to heat. The spring is assumed free of damping, so all energy dissipation in the system takes place in the viscous damper. An external force $f(t)$ is applied to the point mass m. $f(t)$ is considered positive in the same direction as the degree of freedom $x(t)$, which is selected as the displacement from the static state of equilibrium, *i.e.* the gravity force can be ignored. By cutting the mass free from the spring and the damping element, provides that the internal and external dynamic forces are applied as external loads on the mass. The damping and spring force f_d and kx are considered positive in the opposite direction of the external force $f(t)$. Using Newton's 2nd law of motion, the equation of motion for forced vibration of a linear viscous damped SDOF system is given by

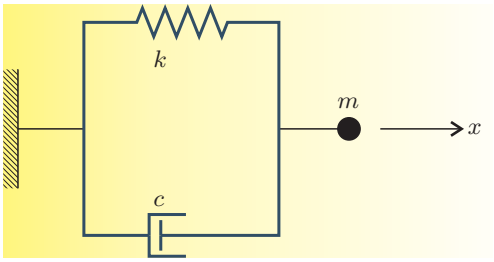

Figure 2–3: Dynamic system with one degree of freedom.

$$-kx - c\dot{x} + f(t) = m\ddot{x} \tag{2–14}$$

Eigenvibrations of Undamped SDOF Systems

For eigenvibrations of an undamped system no external loading is applied, *i.e.* $f(t) = 0$ and no viscous damping exists. According to Eq. (2–14), the governing equation of motion then becomes

$$-kx = m\ddot{x} \tag{2–15}$$

Rewriting of Eq. (2–15 provides

$$\ddot{x} + \omega_0 x = 0 \tag{2–16}$$

The circular eigenfrequency ω_0 included in Eq. (2–16) is given by

$$\omega_0 = \sqrt{\frac{k}{m}} \tag{2–17}$$

The solution of Eq. (2–16) then reads

$$x(t) = A\cos(\omega_0 - \phi), \tag{2–18}$$

where A is the amplitude and ϕ is the phase angle. Eq. (2–18) describes a harmonic motion with the circular eigenfrequency ω_0 determined by Eq. (2–17) . The eigenvibration period becomes

$$T_0 = \frac{2\pi}{\omega_0} = 2\pi\sqrt{\frac{k}{m}} \tag{2–19}$$

The natural frequency f_0 is then

$$f_0 = \frac{1}{T_0} = \frac{1}{2\pi}\omega_0 = \frac{1}{2\pi}\sqrt{\frac{k}{m}} \tag{2–20}$$

Civil engineering structures often have an eigenfrequency f_0 between 0.1Hz to 2.0Hz.

Eigenvibrations of Viscously-Damped SDOF Systems

In case of a damped dynamic system, the viscous damping term is included in the equation of motion with $f(t) = 0$

$$m\ddot{x} + c\dot{x} + kx = 0 \tag{2–21}$$

The damping term is characterised by the so-called damping ratio ζ given by

$$\zeta = \frac{c}{c_0}, \tag{2–22}$$

where c_0 defines the critical damping

$$c_0 = 2\sqrt{km} \tag{2–23}$$

Most civil engineering structures have a damping ratio from 0.01 to 0.05. By use of Eq. (2–17), Eq. (2–22) and Eq. (2–23), the equation of motion for a viscously-damped system can be rewritten

$$\ddot{x} + 2\omega_0\zeta\dot{x} + {\omega_0}^2 x = 0 \tag{2–24}$$

The differential equation specified in Eq. (2–24) can be solved by standard methods and for $\zeta < 1$ the equation of motion is given by

$$x(t) = A\mathrm{e}^{-\alpha t}\left(\frac{\alpha}{\beta}\sin\beta t + \cos\beta t\right) = A\mathrm{e}^{-\alpha t}\sqrt{\frac{1}{1-\zeta^2}}\cos(\beta t - \phi), \tag{2–25}$$

where A is the amplitude to time $t = 0$ determined by initial conditions. The frequency β in Eq. (2–25) is defined by

$$\beta = \omega_0\sqrt{1-\zeta^2} \tag{2–26}$$

The variable α in Eq. (2–25) represents the damping of the system and is given by

$$\alpha = \omega_0\zeta \tag{2–27}$$

The delay of the response $x(t)$ due to the damping is represented by the phase angle ϕ in Eq. (2–25) and is given by

$$\tan\phi = \frac{\zeta}{\sqrt{1-\zeta^2}} \tag{2–28}$$

The response $x(t)$ in Eq. (2–25) is non-periodic due to the factor $\mathrm{e}^{-\alpha t}$, which specifies the decrease of the vibration amplitude with the time. Contrary to an undamped system, the eigenvibrations of a viscously-damped system is characterised by dispersion of energy. The damped eigenvibration period T_d is given by

$$T_\mathrm{d} = \frac{2\pi}{\omega_0\sqrt{1-\zeta^2}} \tag{2–29}$$

With the definition of the damped eigenvibration period T_d, it is possible to establish the damped circular eigienfrequency ω_d

$$\omega_\mathrm{d} = \frac{2\pi}{T_\mathrm{d}} = \omega_0\sqrt{1-\zeta^2} \tag{2–30}$$

At the time t, the motion $x(t)$ is given by Eq. (2–25). At the time $t+nT_\mathrm{d}$ after n damped periods, the motion can be found by use of the definitions in Eq. (2–25), Eq. (2–29) and Eq. (2–30)

$$x(t+nT_\mathrm{d}) = A\mathrm{e}^{-\zeta\omega_0(t+nT_\mathrm{d})}\cos(\omega_\mathrm{d}t+\omega_\mathrm{d}nT_\mathrm{d}-\phi) = \mathrm{e}^{-\zeta\omega_0 nT_\mathrm{d}}x(t) \Rightarrow$$

$$\frac{x(t+nT_\mathrm{d})}{x(t)} = \mathrm{e}^{-\zeta\omega_0 nT_\mathrm{d}} = \mathrm{e}^{-2\pi n\frac{\zeta}{\sqrt{1-\zeta^2}}} \tag{2–31}$$

It means that the motion $x(t)$ at a given time t will decrease with the factor $\mathrm{e}^{-2\pi n\frac{\zeta}{\sqrt{1-\zeta^2}}}$ during the time $t+nT_\mathrm{d}$. In Fig. 2–4 the free vibration characteristic of a damped SDOF system is shown.

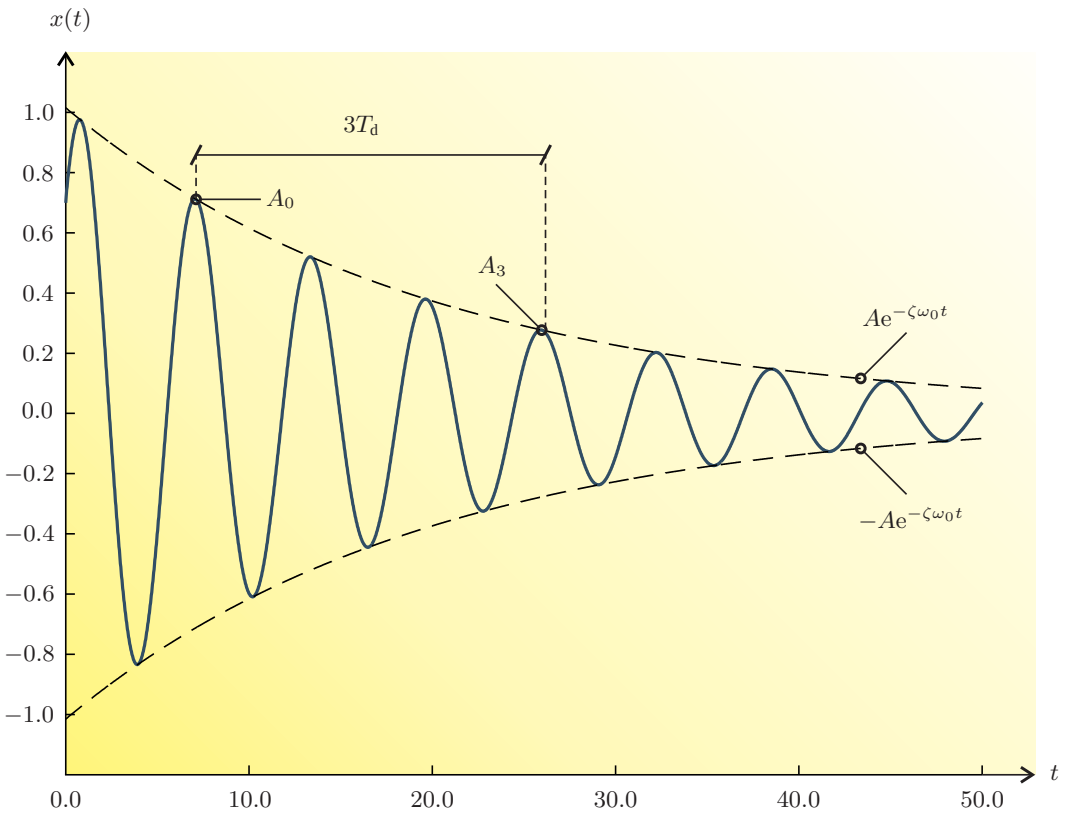

Figure 2–4 Response of a damped system with $\zeta < 1$. After Nielsen (2004).

In order to find the damping ratio ζ the logarithmic decrement δ is presented by use of Eq. (2–31)

$$\delta = \ln\left(\frac{x(t)}{x(t+T_\mathrm{d})}\right) = 2\pi\frac{\zeta}{\sqrt{(1-\zeta^2)}} \tag{2–32}$$

According to Fig. 2–4, the logarithmic decrement δ can be found by observing two upcrossings in the response A_0 and A_n placed with the time interval nT_d

$$\delta = \frac{1}{n}\ln\left(\frac{A_0}{A_n}\right) \tag{2–33}$$

Forced Harmonic Vibrations for SDOF Systems

The equation of motion for forced harmonic vibrations is given by Eq. (2–14). A force excitation $f(t)$ of the following form is assumed

$$f(t) = f_0\cos\omega t, \tag{2–34}$$

where ω is the load frequency. By use of Eq. (2–17), Eq. (2–22) and Eq. (2–23) the equation of motion for forced harmonic vibration reads

$$\ddot{x} + 2\omega_0\zeta\dot{x}\omega_0^2 x = \frac{f_0}{k}\omega_0^2\cos\omega t \tag{2–35}$$

The solution to the inhomogeneous differential equation given by Eq. (2–35) is searched for on the form

$$x(t) = C_1\sin\omega t + C_2\cos\omega t \tag{2–36}$$

Inserting Eq. (2–36) into Eq. (2–35) provides

$$(\omega_0^2-\omega)(C_1\sin\omega t + C_2\cos\omega t) + 2\zeta\omega_0(C_1\cos\omega t - C_2\sin\omega t) = \frac{f_0}{k}\omega_0^2\cos\omega t \tag{2–37}$$

By matching terms with $\sin\omega t$ and $\cos\omega t$, the two arbitrary constants C_1 and C_2 are determined

$$C_1 = \frac{f_0}{k}2\zeta\frac{\omega}{\omega_0}f_1 \tag{2–38}$$

$$C_2 = \frac{f_0}{k}\left(1-(\frac{\omega}{\omega_0})^2\right)f_1, \tag{2–39}$$

where the dynamic amplification factor f_1 is given by

$$f_1 = \sqrt{\frac{1}{\left(1-(\frac{\omega}{\omega_0})^2\right)^2 + \left(2\zeta\frac{\omega}{\omega_0}\right)^2}} \tag{2–40}$$

Inserting Eq. (2–40) into Eq. (2–36) provides

$$x(t) = \frac{f_0}{k}f_1\cos(\omega t - \phi) \tag{2–41}$$

The phase delay of the motion ϕ in Eq. (2–41) can be written in the following way

$$\tan\phi = \frac{2\zeta\frac{\omega}{\omega_0}}{1-(\frac{\omega}{\omega_0})^2} = \frac{2\zeta\omega_0\omega}{\omega_0^2-\omega^2} \tag{2–42}$$

The phase delay ϕ indicates that the maximum motion is observed ϕ later than the maximum loading.

Another way of deriving Eq. (2–41) and Eq. (2–42) is by formulating the force excitation $f(t)$ in complex notation. Eq. (2–34) then reads

$$f(t) = |F|\cos(\omega t-\alpha) = \text{Re}\left(|F|\mathrm{e}^{i(\omega t-\alpha)}\right) = \text{Re}\left(F\mathrm{e}^{i\omega t}\right), \tag{2–43}$$

where

$$F = |F|\mathrm{e}^{-i\alpha} \tag{2–44}$$

In this case the equation of motion for forced vibration is given by

$$\ddot{x}+2\zeta\omega_0\dot{x}+\omega_0^2 x = \text{Re}\left(\frac{f_0}{m}\mathrm{e}^{i\omega t}\right) \tag{2–45}$$

A solution to Eq. (2–45) is searched for on the form

$$x(t) = |X|\cos(\omega t-\phi) = \text{Re}\left(X\mathrm{e}^{i\omega t}\right) = \text{Re}\left(X\mathrm{e}^{i\omega t}\right), \tag{2–46}$$

where

$$X = |X|\mathrm{e}^{-i\phi} \tag{2–47}$$

Inserting Eq. (2–46) into Eq. (2–45) provides

$$\text{Re}\left([m(\omega_0^2-\omega^2+2\zeta\omega_0 i\omega)X-F]\mathrm{e}^{i\omega t}\right) = 0 \tag{2–48}$$

Eq. (2–46) is a possible motion if and only if Eq. (2–48) is fulfilled at all times. This is only possible if the term within the sharp-edged brackets is equal to zero. This leads to

$$X = H(\omega)F, \tag{2–49}$$

where $H(\omega)$ is characterised as the frequency response function

$$H(\omega) = \frac{1}{m(\omega_0^2-\omega^2+2\zeta\omega_0\omega i)} \tag{2–50}$$

It should be noted that $H(\omega)$ is the complex amplitude of $x(t)$ for $F=1$. The denominator in Eq. (2–50) becomes

$$N = m(\omega_0^2-\omega^2+2\zeta\omega_0\omega i) = \left(m\sqrt{(\omega_0^2-\omega_0)^2+4\zeta^2\omega_0^2\omega^2}\right)\mathrm{e}^{i\phi}, \tag{2–51}$$

where ϕ is given by Eq. (2–42). Eq. (2–51) is illustrated graphically in Fig. 2–5. Hence, Eq. (2–49) can be written in the following way

$$X = \frac{|F|}{m\sqrt{\left(\omega_0^2 - \omega^2\right)^2 + 4\zeta^2\omega_0^2\omega^2}} \mathrm{e}^{-i\phi_1} \tag{2–52}$$

where $\phi_1 = \phi + \alpha$. Taken the absolute value of Eq. (2–52) gives

$$|X| = \frac{|F|}{m\omega_0^2\sqrt{\left(1 - \frac{\omega^2}{\omega_0^2}\right)^2 + 4\zeta^2\frac{\omega^2}{\omega_0^2}}} = X_\mathrm{s} f_1, \tag{2–53}$$

where $X_\mathrm{s} = |F|/k$ denotes the amplitude of the motion for a harmonic external load with the amplitude $|F|$ and an infinitely small circular eigenfrequency ω, *i.e.* the inertia and the damping force are ignored. Inserting Eq. (2–53) into Eq. (2–46) provides exactly the same result as stated in Eq. (2–41). As earlier mentioned f_1 is the dynamic amplification factor, which describes the relative increase of the amplitude $|X|$ when the inertia and the damping force have significant influence of the motion. Harmonic excitations with $\omega = \omega_0$ are denoted resonance in which the dynamic amplification factor and the phase angle become $f_1 = 1/2\zeta$ and $\phi = 90°$, respectively. In Fig. 2–6a the dynamic amplification factor f_1 as a function of frequency ratio $\frac{\omega}{\omega_0}$ is shown for different damping ratios ζ. Similarly the phase angle ϕ is shown in Fig. 2–6b.

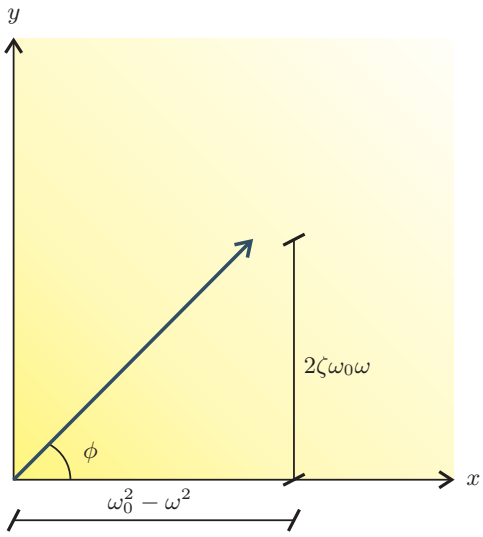

Figure 2–5: Graphic illustration of Eq. (2–51).

2.3.2 Multi Degree of Freedom System Theory

Dynamic systems that require n degrees of freedom specified by n coordinates to describe their motion are called MDOF systems. In general, the force equilibrium of an MDOF system can be established where the inertia forces $\mathbf{M}\ddot{\mathbf{x}}$ are balanced by a set of linear-elastic restoring forces $\mathbf{K}\mathbf{x}$, viscous damping forces $\mathbf{C}\dot{\mathbf{x}}$ and the external force $\mathbf{f}(t)$

$$\mathbf{M}\ddot{\mathbf{x}} + \mathbf{C}\dot{\mathbf{x}} + \mathbf{k}\mathbf{x} = \mathbf{f}(t), \tag{2–54}$$

where $\mathbf{M}$, $\mathbf{C}$ and $\mathbf{K}$ are the mass, damping and stiffness matrices and have the dimensions $n \times n$. $\mathbf{x}(t)$ and $\mathbf{f}(t)$ are $n \times 1$ generalized displacement and force vectors. In case of vibrations due to an arbitrary excitation, the solution to Eq. (2–54) can be described by an impulse response function $\mathbf{h}(\tau)$, also called the weighting function. The function is defined as the output of the system at any time to a unit impulse input applied a time τ before. For zero initial conditions, *i.e.* the displacement vector $\mathbf{x}(0)$ and the velocity vector $\dot{\mathbf{x}}(0)$ are zero, the solution to Eq. (2–54)

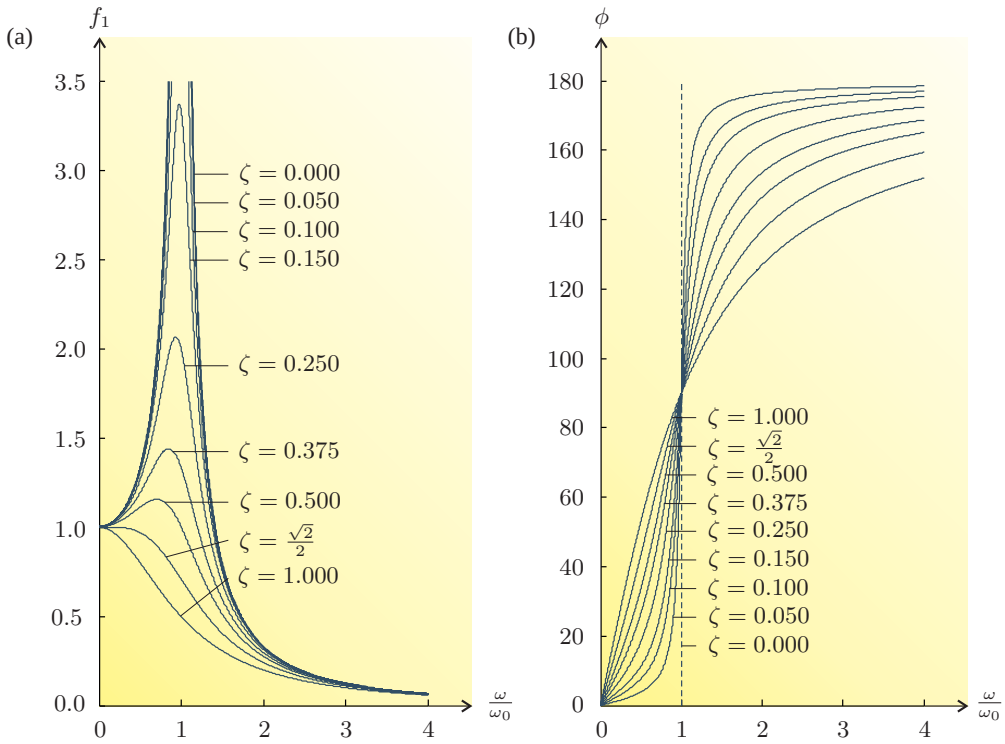

Figure 2–6 Dynamic response as a function of the frequency ratio $\frac{\omega}{\omega_0}$ and the damping ratio ζ: (a) Dynamic amplification factor f_1, (b) Phase angle ϕ. After Nielsen (2004).

can be written in terms of the convolution integral

$$\mathbf{x}(t) = \int_0^\infty \mathbf{h}(\tau)\mathbf{f}(t-\tau)d\tau \tag{2–55}$$

Eq. (2–55) specifies that the response $\mathbf{x}(t)$ is given by a weighted linear sum over the entire history of the input $\mathbf{f}(t)$. The function fully describes the dynamic behaviour of the structural system in the time domain. It is possible to transform Eq. (2–55) into the frequency domain by use of Fourier transformation. The frequency response function $\mathbf{H}(f)$ then reads

$$H(f) = \int_0^\infty h(\tau)\mathrm{e}^{i2\pi f\tau}d\tau \tag{2–56}$$

Letting $\mathbf{F}(f)$ be the Fourier transform of the input $\mathbf{f}(t)$ and letting $\mathbf{X}(f)$ be the Fourier transform of the output $\mathbf{x}(t)$, it follows from Eq. (2–55) that

$$\mathbf{X}(f) = \mathbf{H}(f)\mathbf{F}(f) \tag{2–57}$$

It means that by use of the frequency response function $\mathbf{H}(f)$ and Fourier transform of the input and the output, the convolution integral in Eq. (2–55) reduces to simple algebraic expression in Eq. (2–57). By evaluate the products $\mathbf{x}(t)\mathbf{x}(t+\tau)$ and $\mathbf{f}(t)\mathbf{x}(t+\tau)$ and taking expected values of

both sides, the autocorrelation function $\mathbf{R}_{\text{ff}}$ and cross-correlation function $\mathbf{R}_{\text{xf}}$ as function of the impulse response function $\mathbf{h}(\tau)$ can be found. Direct Fourier transformation of these correlation functions together with various algebraic steps, give the important formulas for the two-sided spectral density functions $\mathbf{S}_{\text{xx}}$ and $\mathbf{S}_{\text{xf}}$ and the one-sided spectral density functions $\mathbf{G}_{\text{xx}}$ and $\mathbf{G}_{\text{xf}}$

$$\mathbf{S}_{\text{xx}} = |\mathbf{H}(f)|^2 \mathbf{S}_{\text{ff}}(f) \tag{2–58a}$$

$$\mathbf{S}_{\text{xf}} = \mathbf{H}(f)\mathbf{S}_{\text{ff}}(f) \tag{2–58b}$$

$$\mathbf{G}_{\text{xx}} = |\mathbf{H}(f)|^2 \mathbf{G}_{\text{ff}}(f) \tag{2–59a}$$

$$\mathbf{G}_{\text{xf}} = \mathbf{H}(f)\mathbf{G}_{\text{ff}}(f) \tag{2–59b}$$

For further details, see Bendat and Piersol (2000).

Modal Analysis of MDOF Systems

The following section describes the theory of determining the modal properties of an MDOF dynamic system. Assuming that the structural system is given a unit impulse and then left on its own, the differential equation for undamped vibrations of an MDOF system follows from Eq. (2–54) for $\mathbf{C} = 0$ and $\mathbf{f}(t) = 0$:

$$\mathbf{M}\ddot{\mathbf{x}} + \mathbf{k}\mathbf{x} = \mathbf{0} \tag{2–60}$$

The solution to Eq. (2–60) is sought on the form

$$\mathbf{x}(t) = \text{Re}\left(\mathbf{\Phi}\text{e}^{i\omega t}\right) \tag{2–61}$$

The vector $\mathbf{\Phi}$ in Eq. (2–61) is an unknown complex amplitude vector. Inserting Eq. (2–61) into Eq. (2–60) provides, when same arguments are used as in Eq. (2–48),

$$\text{Re}\left([(i\omega)^2\mathbf{M}\mathbf{\Phi} + \mathbf{K}\mathbf{\Phi}]\text{e}^{i\omega t}\right) = \mathbf{0} \Rightarrow$$

$$\left(\mathbf{K} - \omega^2\mathbf{M}\right)\mathbf{\Phi} = \mathbf{0} \tag{2–62}$$

Eq. (2–62) represents a homogeneous system of n linear equations for the determination of the circular eigenfrequency ω and the unknown amplitude $\mathbf{\Phi}$. The necessary condition for non-trivial solutions $\mathbf{\Phi} \neq \mathbf{0}$ is

$$\det\left(\mathbf{K} - \omega^2\mathbf{M}\right) = 0 \tag{2–63}$$

Eq. (2–63) is denoted the frequency condition. For each of the roots $\omega_1^2, \omega_2^2, \ldots, \omega_{\text{n}}^2$, which forms the eigenvalues of Eq. (2–63), a non-trivial solution $\mathbf{\Phi}^{(1)}, \mathbf{\Phi}^{(2)}, \ldots, \mathbf{\Phi}^{(\text{n})}$ exists to Eq. (2–63). These solutions are denoted the undamped eigenmodes. Given the circular eigenfrequencies $\omega_{\text{j}} = \sqrt{\omega_{\text{j}}^2}$ and the mode shapes $\mathbf{\Phi}^{(\text{j})}$, Eq. (2–61) can be written in the following way

$$\mathbf{x}(t) = \text{Re}\left(\mathbf{\Phi}^{(\text{j})}\text{e}^{i\omega_{(\text{j})}t}\right) = \mathbf{\Phi}^{(\text{j})}\text{Re}\left(\text{e}^{i\omega_{\text{j}}t}\right) = \mathbf{\Phi}^{(\text{j})}\cos\omega_{\text{j}}t \tag{2–64}$$

However, it can be shown that $\mathbf{x}(t) = \mathbf{\Phi}^{(\mathrm{j})} \sin \omega_{\mathrm{j}} t$ also is a solution to Eq. (2–60). $2n$ linear independent solutions to the homogeneous differential equation formulated in Eq. (2–60) then exist

$$\left.\begin{array}{l} \mathbf{x}(t) = \mathbf{\Phi}^{(\mathrm{j})} \cos \omega_{\mathrm{j}} t \\ \mathbf{x}(t) = \mathbf{\Phi}^{(\mathrm{j})} \sin \omega_{\mathrm{j}} t \end{array}\right\} = j = 1, \ldots, n \tag{2–65}$$

Thus, any solution to Eq. (2–60) can be written as a linear combination of the fundamental solutions in Eq. (2–65)

$$\mathbf{x}(t) = a_1 \mathbf{\Phi}^{(1)} \cos \omega_1 t + \cdots + a_{\mathrm{n}} \mathbf{\Phi}^{(\mathrm{n})} \cos \omega_{\mathrm{n}} t + b_1 \mathbf{\Phi}^{(1)} \sin \omega_1 t + \cdots + b_{\mathrm{n}} \mathbf{\Phi}^{(\mathrm{n})} \sin \omega_{\mathrm{n}} t \tag{2–66}$$

The task is now to determine the coefficients a_1, a_2,..., a_{n} and b_1, b_2,..., b_{n}, so the initial conditions $\mathbf{x}_0$ and $\dot{\mathbf{x}}_0$ are fulfilled

$$\mathbf{x}(0) = \mathbf{x}_0 = \mathbf{\Phi}^{(1)} a_1 + \mathbf{\Phi}^{(2)} a_2 + \cdots + \mathbf{\Phi}^{(\mathrm{n})} a_{\mathrm{n}} \Rightarrow$$

$$\mathbf{x}_0 = \mathbf{P}\mathbf{a} \Rightarrow \mathbf{a} = \begin{bmatrix} a_1 \\ a_2 \\ \vdots \\ a_{\mathrm{n}} \end{bmatrix} = \mathbf{P}^{-1} \mathbf{x}_0, \tag{2–67}$$

where $\mathbf{P} = \left[\mathbf{\Phi}^{(1)}, \ldots, \mathbf{\Phi}^{(\mathrm{n})}\right]$ is denoted the modal matrix.

$$\dot{\mathbf{x}}(0) = \dot{\mathbf{x}}_0 = \mathbf{\Phi}^{(1)} b_1 \omega_1 + \mathbf{\Phi}^{(2)} b_2 \omega_2 + \cdots + \mathbf{\Phi}^{(\mathrm{n})} b_{\mathrm{n}} \omega_{\mathrm{n}} \Rightarrow$$

$$\dot{\mathbf{x}}_0 = \mathbf{P}\mathbf{b}\omega \Rightarrow \mathbf{b}\omega = \begin{bmatrix} b_1 \omega_1 \\ b_2 \omega_2 \\ \vdots \\ b_{\mathrm{n}} \omega_{\mathrm{n}} \end{bmatrix} = \mathbf{P}^{-1} \dot{\mathbf{x}}_0 \tag{2–68}$$

2.4 Digital Data Analysis Processing

Before an experimental modal analysis can be established, some specific data acquisition and processing procedures are required. In general, an experimental modal analysis involves instrumentation by transducers. Transducers like accelerometers consist of a mechanical element that get stressed by accelerative forces, which causes an electrical charge that is proportional to the accelerative forces. The output from the individual transducer consists of an analog signal, which means that the signal is continuously variable. When dealing with data analysis, the most desirable way to store data is in a digital medium that is easily accessed by a computer. For that reason the analog signals from the transducers must be converted into a digital format using an analog-to-digital converter. The signals will then be represented by discrete values. In Fig. 2–7 the process prior to the digital signal processing is shown. According to Fig. 2–7 the input signal is processed with an electronic anti-aliasing low-pass filter. The reason for this low-pass filter is described in the following section. The section is based on Smith (1997) and Ewins (2000).

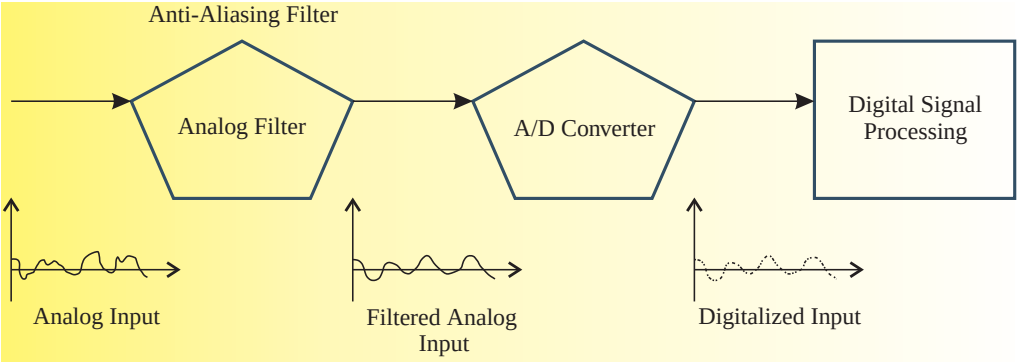

Figure 2–7 Schematic diagram of an analog-to-digital conversion of analog signal. After Smith (1997).

2.4.1 Sample Frequency and Aliasing

Determination of an appropriate sampling frequency f_s is important for digital data analysis. Fig. 2–8 shows two sinusoidal waves before and after digitization. The continuous line represents the analog signal entering the analog-to-digital converter, while the doted line are the digital signal leaving the analog-to-digital converter. The sine wave in Fig. 2–8a has a frequency of 0.09 of the sampling frequency f_s. Because no other sinusoid will produce the pattern of samples, the samples properly represent the analog signal. However, when the analog frequency is increased to 0.95 of the sampling frequency f_s, the samples represent a different sine wave from the one contained from the analog signal data. This is shown in Fig. 2–8b. Sinusoids changing frequencies during sampling is denoted as aliasing. In order to avoid this phenomenon, the Nyquist sampling theorem is used, which specifies that a continuous signal can be properly sampled only if it does not contain frequency components above one-half of the sampling frequency f_s. This frequency is denoted the Nyquist frequency, or the aliasing frequency, and can be formulated by use of the sampling duration T_0 and the total number of samples n

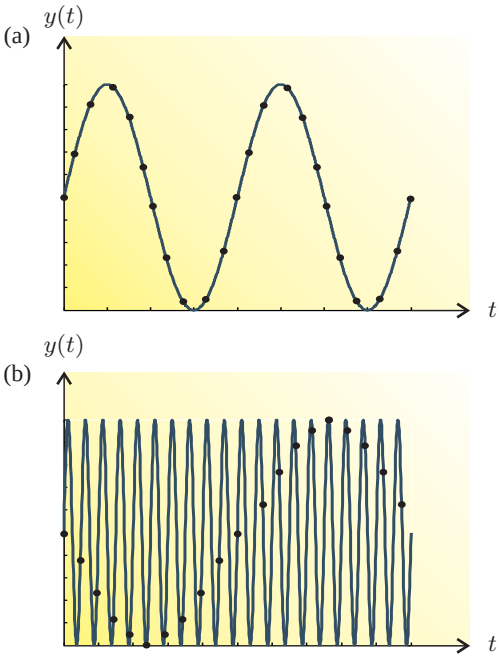

Figure 2–8: Sinusoid before and after digitization: (a) Proper sampling with a frequency of an analog sine wave smaller than the Nyquist frequency, (b) Improper sampling with a frequency of an analog sine wave greater than the Nyquist frequency. After Smith (1997).

$$f_{\text{nyquist}} = f_{\frac{n-1}{2}} = \frac{\frac{n-1}{2}}{T_0} = \frac{\frac{n-1}{2}}{(n-1)\frac{1}{f_s}} = \frac{1}{2\frac{1}{f_s}} = \frac{f_s}{2} \tag{2–69}$$

The Nyquist frequency f_{nyquist} is the highest frequency that can be defined by a sampling frequency f_{s}. Frequencies in the original data above f_{nyquist} will appear below f_{nyquist} and be confused with the data in this lower-frequency range. A low-pass filter is for that reason used to remove the frequency content of the original data above f_{nyquist} prior to the analog-to-digital conversion. Such a filter is referred to as an anti-aliasing filter. Because no low-pass filter has an infinitely sharp cut-off shape, the anti-aliasing filter cut-off frequency is set to approximately 80 % of f_{nyquist} to assure that any data at frequencies above f_{nyquist} are strongly suppressed. The aliasing phenomenon is shown in Fig. 2–9. A good rule of thumb for experimental modal analysis is that if the lowest frequency of interest is f_{min}, then the length of the time series should at least be 1000 cycles of the corresponding period. With this mind and the above definition of an anti-aliasing filter, the following expressions can be stated:

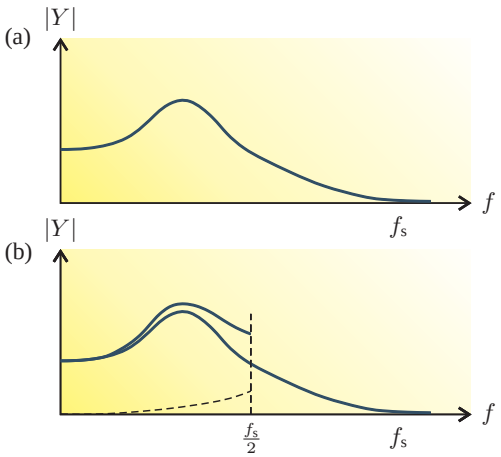

Figure 2–9: Aliasing after Fourier transform: (a) True spectrum of signal, (b) Indicated spectrum from FFT. After Ewins (2000).

$$t_{\text{total}} \geq \frac{x}{f_{\text{min}}}, \quad x \approx 1000 \tag{2–70a}$$

$$f_{\text{max}} \leq 0.8 f_{\text{nyquist}} \Rightarrow f_{\text{s}} \geq 2.5 f_{\text{max}}, \tag{2–70b}$$

where f_{max} is the highest frequency of interest.

2.4.2 Leakage Caused by Fourier Transform

Traditional experimental modal analysis is based on Fourier transform techniques. The Fourier transform of digital data is usually obtained by Fast Fourier Transformation FFT, which can be used to provide estimates of spectral density and correlation functions. However, FFT assumes periodicity, which means that the data record of finite length is assumed to repeat itself in both ends of the record. Due to the fact that digital signals in general exhibit nonperiodicity, errors will be introduced. These errors are denoted leakage and can be illustrated by Fig. 2–10, in which two sinusoidal signals are represented. In Fig. 2–10a the signal is perfectly periodic in the time window T, which induces a single line in the spectrum. In Fig. 2–10b the periodicity assumption is not valid. As a result, the spectrum is not represented by a single line. Instead, energy has leakage into a number of spectral lines close to the true frequency. For modal analysis this means that the energy related to vibrations at the resonance frequencies leaks out, which results in an apparent higher damping of the corresponding modes.

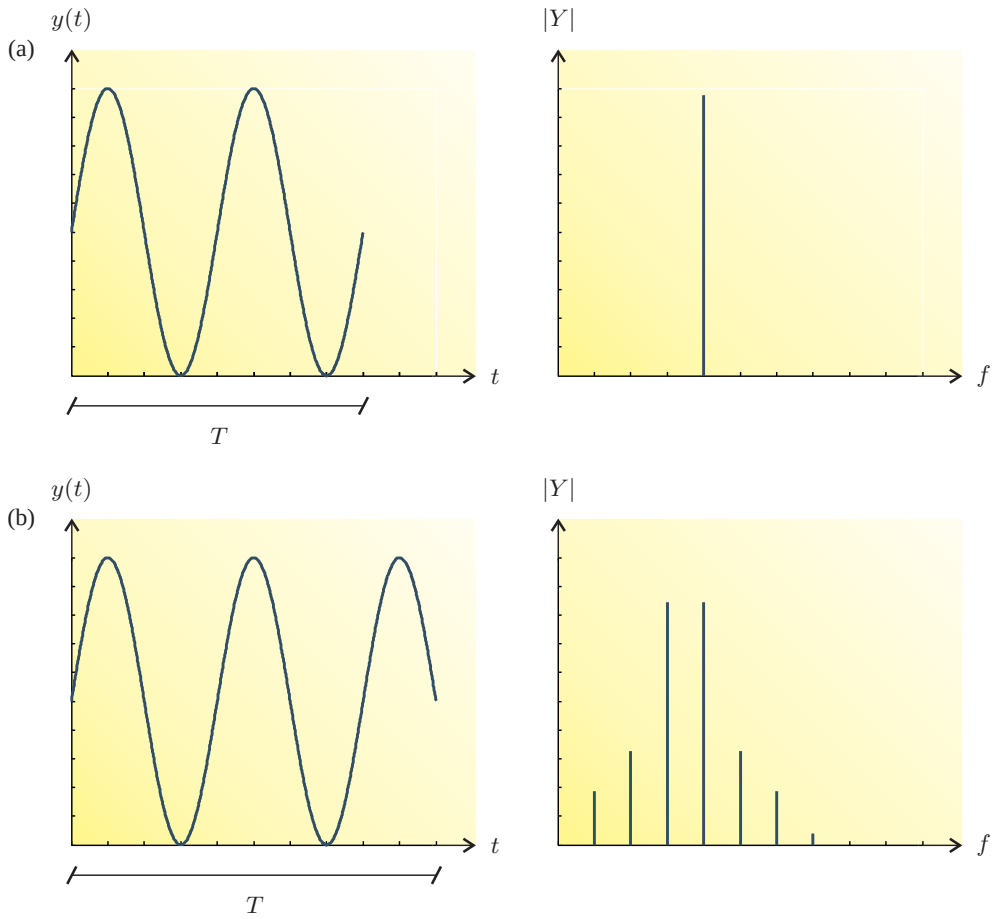

Figure 2–10 Sample length and leakage of frequency spectrum: (a) Ideal signal, (b) Non-periodic signal. After Ewins (2000).

Windowing

A solution to leakage is by windowing the data before the FFT is applied and thereby secure periodicity by multiplying the measured data by a suitable time window. The widely used cosine-taper data window for digital data signals reads

$$d(t) = \begin{cases} \frac{1}{2}\left(1 - cos\frac{10\pi t}{T_0}\right) & \text{for} \quad 0 \leq t \leq \frac{T_0}{10} \\ 1.004 & \text{for} \quad \frac{T_0}{10} \leq t \leq \frac{9T_0}{10} \\ \frac{1}{2}\left(1 + cos\frac{10\pi(t-\frac{9T_0}{10})}{T_0}\right) & \text{for} \quad \frac{9T_0}{10} \leq t \leq T_0 \end{cases} \tag{2–71}$$

In Fig. 2–11 the cosine-taper window is illustrated.

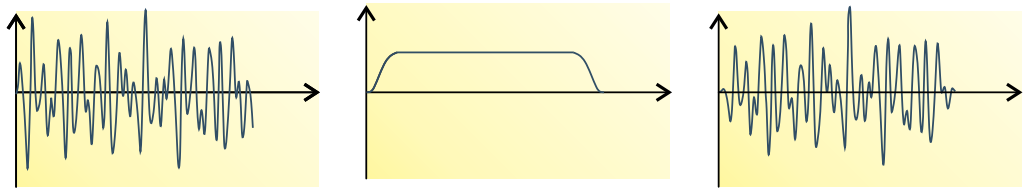

Figure 2–11 Use of cosine-taper window in order to secure periodicity. After Liu and Frigaard (2001).

In many cases the frequency spectrum provided by an FFT analysis will be filled with noise, because of insufficient information in the original data to obtain a well defined spectrum. To reduce the noise, averaging is applied. This is done by dividing the data into n multiple sub segments, multiply each of the segments with the time window and convert them into a frequency spectrum. The resulting spectrum is then found by summing all the spectra from each sub segment and dividing by the number of sub segments n. Using 8 sub segments will for that reason results in a reduction of the standard deviation for each spectral from 100 % to $\frac{1}{\sqrt{8}} = 35\%$. However, it should be noted that the frequency resolution will be more coarse when averaging.

2.5 Summary

As stated in the introduction, the theory explained in this chapter will serve as a foundation for applications of experimental modal analysis in the subsequent chapter. The main results of the chapter are listed below.

System identification is able to establish mathematical models of a dynamic system calibrated from measured data by use of statistical methods.

Experimental modal analysis is a method used to determine the dynamic properties of a structure. In a controlled environment it may be possible to measure the input loading and the output response, which means that the modal properties can be found by fitting a model to the frequency response function. This method is referred to as input-output modal identification. However, it can be difficult to measure the input loading of large civil engineering structures under operational conditions. In this situation output-only modal identification is used, where the modal properties are estimated by simple peak picking.

Random processes or stochastic processes $\{x_{\mathrm{k}}(t)\}$ consist of several single time histories $x_{\mathrm{k}}(t)$, also referred to as sample functions.

Stationary random process is characterised by a time-invariant loading and structural system. In this case the mean value $\mu_x(t_1)$ and autocorrelation $R_{\mathrm{xx}}(t_1, t_1 + \tau)$ for a random process $\{x(t)\}$ remain constant, even though changes in the time t_1 take place.

Autocorrelation functions are a measure of time-related properties in the data that are separated by fixed time delays. For a single time history record $x_{\mathrm{k}}(t)$ from a stationary random process $\{x_{\mathrm{k}}(t)\}$, the autocorrelation function $R_{\mathrm{xx}}(\tau, k)$ can be found by delaying the record relatively to itself by some fixed time delay τ and multiplying the original record with the delayed record. The resulting product is averaging over the record length.

Cross-correlation functions are a measure of the similarity between a time history record $x_{\mathrm{k}}(t)$ from a stationary random process $\{x_{\mathrm{k}}(t)\}$ and a time history record $y_{\mathrm{k}}(t)$ from a stationary random process $\{y_{\mathrm{k}}(t)\}$ with a fixed time delay τ. Multiplying the two time history records from each random process and averaging over the record length, produce the cross-correlation function.

Spectral density functions represent the data in the frequency domain. They can be found by the Fourier transform of the correlation functions. Another way of defining the spectral density functions is by use of Fourier transform on the original data records.

Resonance frequency occurs when the circular frequency of harmonic excitations becomes equal to the circular eigenfrequency of the structure. In this case the dynamic amplification factor increases drastic. The magnitude of the dynamic amplification factor depends on the structural damping in the system.

Analog-to-digital converter is a device that converts the analog signal from transducers into a digital format that can be accessed by computers.

Nyquist frequency or the aliasing frequency f_{nyquist} is the maximum frequency that a digital signal can contain.

Aliasing is a phenomenon that will occur when dealing with frequencies in the original data higher than the Nyquist frequency f_{nyquist}. In this situation the frequencies above the f_{nyquist} will appear reflected or aliased below f_{nyquist}.

Leakage is a problem for frequency analysis, which is a direct consequence of the use of Fourier transform techniques. These techniques assume that the finite data record of length repeats itself in both ends of the record. As real measurements exhibit nonperiodicity some energy will leak out of the original signal spectrum into other frequencies.

Windowing can be used to avoid leakage. By multiplying the measured data by a suitable taper data window, periodicity is secured.

CHAPTER 3
Structural Assessment by Operational Modal Identification

In order to determine the dynamic properties of civil engineering structures, modal analysis is performed. In general, the structural dynamic properties, or modal parameters, can be estimated by using either analytical, numerical or experimental methods. However, a correct estimate of the structural properties based on pure physics and fundamental laws is often difficult for large civil engineering structures such as bridges, tall buildings and wind turbines. In these cases it can be justified to conduct modal testing in order to support calibrating, updating and validating computational models used in the design stage. This chapter presents a thorough evaluation of operational modal analysis with focus on the theory and its application. In addition, a literature review of operational modal identification on wind turbines will take place. Firstly, however, a short introduction to experimental modal analysis is given.

3.1 Introduction to Experimental Modal Analysis

Modal analysis is a method to describe a structure in terms of its natural characteristics. The natural characteristics of the structure, also denoted as its dynamic properties, are the resonance frequency ω, the damping ratio ζ and the mode shape $\mathbf{\Phi}$. The resonance frequency is the frequency at which any excitation produces an exaggerated response. This is a very important parameter to know, since excitation close to the resonance frequency involves excessive vibration, which may cause fatigue failure or in extreme cases complete structural failure. Sufficient damping provided in the entire structure is in that connection crucial in order to counteract the strong amplifications when the structure is dynamically loaded near the resonance frequencies. Since the very early days of awareness of structural vibrations, experimental modal analysis has been necessary for two major objectives:

1. Validating of numerical modal analysis through comparison of numerical results with those obtained from experimental modal analysis. This process is called modal updating.

2. After the event of a natural phenomenon such as a windstorm, experimental modal analysis is helpful to evaluate whether or not structural damage has occurred. In other words, estimates of dynamic properties of a structure during its service life can be determined by experimental modal testing.

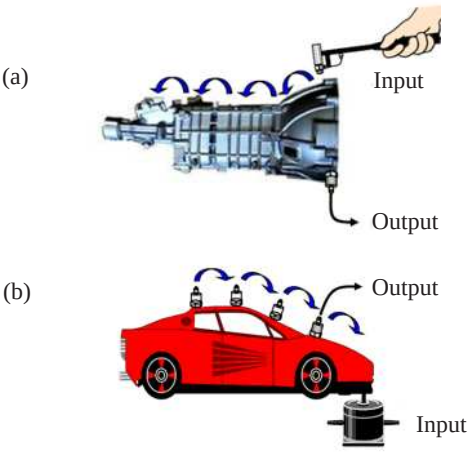

Figure 3–1: Traditional modal technology: (a) Hammer excitation, (b) Shaker excitation. After Andersen (2011).

In the traditional experimental modal technology a set of frequency response functions at several points along the structure are estimated from the measured response divided by the measured excitation, see Eq. (2–57). A popular method of exciting structures artificially is through use of an impulse hammer: This device has the advantages of providing almost white noise, *i.e.* the spectral density function of the impulse loading is almost constant over all frequencies. It means that the output spectrum contains full information of the structure as all modes are excited equally. By move the excitation and only measure the response in one single point, it is possible to determine the frequency response function matrix $\mathbf{H}(\omega)$. This procedure is called multi input single output (MISO). The ratio between the individual entries in the frequency response function $\mathbf{H}(\omega)$ for a frequency ω equal to the resonance frequency ω_0 represents the corresponding mode shape $\mathbf{\Phi}$. An alternative to impulse hammers is electrodynamic shakers, which often is used to excite large and complex structures like cable bridges. The shaker device is able to produce a large variety of input signals like random and multi-sine signals. Due to the possibility of applying sinusoidal forces, a direct identification of the resonance frequencies and mode shapes is easy. For this type of modal procedure the frequency response function is found by moving accelerometers with one or more fixed accelerometers as reference and only excite the structure in one single point. This procedure is called single input multi output (SIMO). The two procedures of determining the dynamic properties of an arbitrary structure are shown in Fig. 3–1. However, the main problem with forced vibration tests on large civil engineering structures is that the most significant modes of vibration in a low range of frequencies are difficult to excite. Moreover, forced excitation of such structures requires extremely heavy excitation equipment. As a consequence of the drawbacks related to traditional experimental modal analysis, operational modal identification is developed. This method allows to determine the inherent properties of a structure by measuring only the response of the structure without using an artificial excitation. In the following section a more detail description of operational modal analysis is given.

3.2 Operational Modal Identification

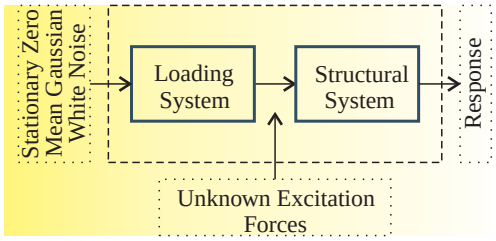

Figure 3–2: Principle of operational modal analysis. After Gade *et al.* (2005).

In many cases large civil engineering structures are excited by natural loads that cannot easily be controlled, for instance wave loads, wind loads or traffic loads. Besides, the structures are excited by noise from environmental vibrations around the structure. Thus, a procedure to identify modal parameters based on the output response is needed. Instead of exciting the structure artificially and dealing with the natural excitation as an unwanted noise source, operational modal identification uses the natural excitation as the excitation source. This means that the dynamic properties of the structure are determined within true boundary conditions and actual force and vibration levels. Operational modal identification makes use of the multiple input multi output (MIMO) technology. Contrary to traditional experimental modal analysis, closely space modes and repeated modes are easily determined by this identification method with a high degree of accuracy. Fig. 3–2 shows the principle of operational modal analysis. The unknown excitation forces are assumed to be produced by a virtual system loaded by stationary zero mean Gaussian white noise. This white noise is assumed to drive both the real structural system and the virtual loading system. It means that modes belonging to the real structural system and "modes" that belong to the virtual loading system are identified. The real structural modes are characterised as lightly damped modes, whereas the virtual loading "modes" are characterised as highly damped "modes". In addition, identification of computational modes might be discovered, because the signals are contaminated with noise. In general this means that it is of outmost importance that the structural modes are separated from the noise modes and excitation modes during the modal identification process.

Different methods of identifying the structural modal parameters exist in operational modal analysis. Frequency Domain Decomposition (FDD) identification techniques and Stochastic Subspace Identification (SSI) are widely used. However, in the following only the frequency domain identification is presented.

3.2.1 Frequency Domain Decomposition Technique

In order to to determine the damped eigenfrequency ω_d, the damping ratio ζ and the damped mode shape $\mathbf{\Phi}^{(j)}$ of a civil engineering structure, the FDD technique is useful. This section explains how the spectral density matrix for each output time series is decomposed into a set of single-degree-of-freedom systems and how the individual SDOF autospectral density functions are transfered back to time domain to identify the damped eigenfrequency ω_d and the damping ratio ζ for each SDOF system. The section is based on Brincker *et al.* (2000), Zang *et al.* (2001) and Brincker *et al.* (2001).

Theoretical Overview of Frequency Domain Decomposition

According to Eq. (2–59a), the output spectral density matrix $\mathbf{G}_{yy}(\omega)$ is described by the input spectral density matrix $\mathbf{G}_{xx}(\omega)$ and the frequency response matrix $\mathbf{H}(\omega)$

$$\mathbf{G}_{yy}(\omega) = \overline{\mathbf{H}}(\omega)\mathbf{G}_{xx}(\omega)\mathbf{H}(\omega)^{T}, \tag{3–1}$$

where the bar over $\mathbf{H}$ indicates the complex conjugated and the superscript T denotes transpose. The frequency response matrix $\mathbf{H}(\omega)$ defined by Eq. (2–56) can be written in a typical partial fraction form in terms of poles λ_k and residues $\mathbf{R}_k$

$$\mathbf{H}(i\omega) = \sum_{k=1}^{n} \frac{\mathbf{R}_k}{i\omega - \lambda_k}, \tag{3–2}$$

where n is the number of modes of interest. The poles λ_k is the modal participation factor, which specifies how much a given mode $\mathbf{\Phi}^{(j)}$ participates in a given direction. The modal participation factor λ_k is given by

$$\lambda_k = \frac{\mathbf{\Phi}^{(j)T}\mathbf{M}\mathbf{U}}{\mathbf{\Phi}^{(j)T}\mathbf{M}\mathbf{\Phi}^{(j)}}, \tag{3–3}$$

where $\mathbf{M}$ and $\mathbf{U}$ are the mass matrix and influence vector, respectively. The residue $\mathbf{R}_k$ is then given by

$$\mathbf{R}_k = \mathbf{\Phi}_k\lambda_k \tag{3–4}$$

By assuming that the input $x(t)$ is white noise, *i.e.* the input spectral density matrix $\mathbf{G}_{xx}(\omega)$ is constant, Eq. (3–1) then becomes

$$\mathbf{G}_{yy}(\omega) = \sum_{k=1}^{n}\sum_{s=1}^{n}\left[\frac{\mathbf{R}_k}{i\omega - \lambda_k} + \frac{\overline{\mathbf{R}}_k}{i\omega - \overline{\lambda}_k}\right]\mathbf{C}\left[\frac{\mathbf{R}_s}{i\omega - \lambda_s} + \frac{\overline{\mathbf{R}}_s}{i\omega - \overline{\lambda}_s}\right]^{H}, \tag{3–5}$$

where $\mathbf{C}$ is the constant input spectral density matrix and the superscript H denotes complex conjugated and transpose. Using the Heaviside partial fraction theorem and furthermore assuming a lightly damped structure and that only a limited number of modes at a certain frequency ω contributes, the output spectral density function $\mathbf{G}_{yy}(\omega)$ can be written in the following final form

$$\mathbf{G}_{yy}(\omega) = \sum_{k\in \mathrm{Sub}(\omega)}^{n} \frac{\mathbf{d}_k\mathbf{\Phi}_k\mathbf{\Phi}_k^{T}}{i\omega - \lambda_k} + \frac{\overline{\mathbf{d}}_k\overline{\mathbf{\Phi}}_k\overline{\mathbf{\Phi}}_k^{T}}{i\omega - \overline{\lambda}_k}, \tag{3–6}$$

where $\mathbf{d}_k$ is a scalar constant and k$\in$Sub(ω) is the set of modes that contribute at the particular frequency.

Identification Procedure

The FDD method is an extension of the well-known frequency domain approach, also referred to as the peak picking approach, that is based on mode estimation directly from the autospectral density matrix at the peak. Four main steps are needed in order to find the damped eigenfrequency ω_d and the damping ratio ζ by use of the FDD technique.

1. A Discrete Fourier Transform (DFT) is performed on the raw output time data $y(t)$ in order to obtain the spectral density matrix $\mathbf{G}_{\mathrm{yy}}(\omega)$ known at discrete frequencies.

2. Estimation of each output spectral density matrix is decomposed by taking the Singular Value Decomposition (SVD) of the matrix, *i.e.* a unitary matrix holding singular vectors and a diagonal matrix holding scalar singular values are defined.

3. Near a peak corresponding to the k th mode in the spectrum the first singular vector is an estimate of the mode shape and the corresponding singular value is the autospectral density function corresponding to a SDOF system. This function is identified by use of the Modal Assurance Criterion (MAC).

4. By use of Inverse Fourier Transform (IFFT) on the autospectral density function the damped eigenfrequency ω_{d} and the damping ratio ζ are estimated from the correlation function.

Basically, the dynamic deflection $\mathbf{y}(t)$ of a damped MDOF system is a linear combination of the mode shapes $\mathbf{\Phi}^{(\mathrm{j})}$ and the modal coordinates $\mathbf{q}(t)$ according to Eq. (2–66)

$$\mathbf{y}(t) = \mathbf{\Phi}\mathbf{q}(t) = \sum_{j=1}^{n} \mathbf{\Phi}^{(\mathrm{j})}\mathbf{q}_{\mathrm{j}}(t) \tag{3–7}$$

Eq. (3–7) is illustrated graphically in Fig. 3–3.

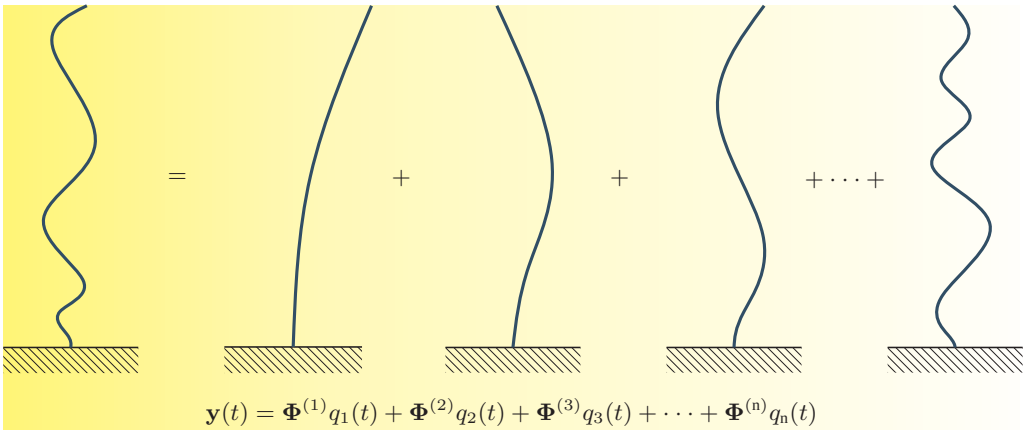

Figure 3–3 System response $\mathbf{y}(t)$ as a linear combination of the mode shapes $\mathbf{\Phi}^{(\mathrm{j})}$ and the modal coordinates $\mathbf{q}_{\mathrm{j}}(t)$. After Andersen (2011).

According to Eq. (2–2) the correlation function of the system response $\mathbf{y}(t)$ then reads

$$\mathbf{R}_{\mathrm{yy}}(\tau) = \mathrm{E}\left[\mathbf{y}(t+\tau)\mathbf{y}(t)^{\mathrm{T}}\right] = \mathrm{E}\left[\mathbf{\Phi}\mathbf{q}(t+\tau)\mathbf{q}(t)^{\mathrm{H}}\mathbf{\Phi}^{\mathrm{H}}\right] = \mathbf{\Phi}\mathbf{R}_{\mathrm{qq}}(\tau)\mathbf{\Phi}^{\mathrm{H}} \tag{3–8}$$

By use of Fourier transformation, the spectral density functions can be obtained

$$\mathbf{G}_{\mathrm{yy}}(f) = \mathbf{\Phi}\mathbf{G}_{\mathrm{qq}}(\mathrm{f})\mathbf{\Phi}^{\mathrm{H}} \tag{3–9}$$

As earlier mentioned the first step in the FDD technique is to determine the output spectral density matrix for each frequency by use of a Discrete Fourier Transform. In general, the size of

each spectral density matrix is $n \times n$, where n is the number of transducers. Each element of the matrices is a spectral density function. The diagonal elements of the matrices are the real valued spectral densities between a response and itself, *i.e.* the autospectral density. The off-diagonal elements are the complex cross spectral density between two different responses. It is important to notice, that the spectral density matrix is Hermitian which means that it is complex conjugated symmetric, see Section 2.2.2. To avoid too much redundant information when estimating the spectral densities, a proper choice of projection channels are used. Often many row and columns in the spectral density matrix are linear combinations of the others. In case of a single test setup the projection channels are found by determining the correlation coefficient of the measured data. The idea is to find the channel that correlates most with other channels. This channel most likely contains maximum physical information

$$w_{\mathrm{i}} = \sum_{i=1}^{n} = |C_{\mathrm{ij}}|\,, \tag{3–10}$$

$$\text{Find max}\,([w_1, w_2, ..., w_{\mathrm{n}}]) \tag{3–11}$$

where n is the number of channels and j$\neq$i. The remaining number of requested projection channels are found by similar search of the correlation coefficient matrix as channels that correlate the least with all previous found projection channels. These channels bring most new information.

According to the theory of the FDD technique the Hermitian spectral density matrix known at discrete frequencies is decomposed by taking the Singular Value Decomposition of the matrix

$$\mathbf{G}_{\mathrm{yy}}(\omega_{\mathrm{i}}) = \mathbf{U}_{\mathrm{i}}\mathbf{S}_{\mathrm{i}}\mathbf{U}_{\mathrm{i}}^{\mathrm{H}}, \tag{3–12}$$

where the matrix $\mathbf{U}_{\mathrm{i}} = [\mathbf{u}_{\mathrm{i1}}\mathbf{u}_{\mathrm{i2}} \cdots \mathbf{u}_{\mathrm{in}}]$ is an unitary matrix containing n singular vectors $\mathbf{u}_{\mathrm{ij}}$ that are orthogonal to each other and $\mathbf{S}_{\mathrm{i}}$ is a singular value diagonal matrix holding the singular values s_{ij}. The singular values s_{ij} and the singular vectors $\mathbf{u}_{\mathrm{ij}}$ are ordered in singular value descending order, *i.e.* the first singular value is the largest. Comparing Eq. (3–9) with Eq. (3–12), it can be understood that the singular vectors $\mathbf{u}_{\mathrm{ij}}$ serve estimations of the mode shapes and the corresponding singular values s_{ij} present the response of each of the modes (SDOF system) expressed by the spectrum of each modal coordinate. It is then assumed that $\mathbf{G}_{\mathrm{qq}}$ is a diagonal matrix and the modes shapes $\mathbf{\Phi}^{(\mathrm{j})}$ are orthogonal.

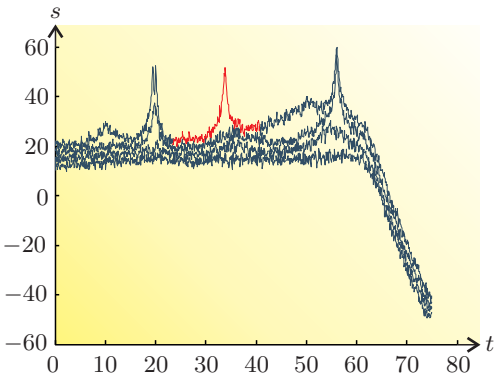

Figure 3–4: Example of singular values of the spectral density matrix.

If only the k th mode is dominating, Eq. (3–6) only consists of one term and for that reason the first singular vector $\mathbf{u}_{\mathrm{ij}}$ is an estimate of the mode shape. The corresponding first singular value s_{ij} is the autospectral density function of the corresponding SDOF system. If more than one time record is performed, the singular value for each time record is averaged. It means that the pick picking is based on the average singular values. An illustration of the singular values of the output spectral density matrix is shown in Fig. 3–4. In the FFD technique only the resonance frequency is estimated of the picked modes, which results in a damping ratio of 0. The Enhanced Frequency

Domain Decomposition (EFDD) technique is an extension to the FDD technique. Compared to FDD, the EFDD technique gives an improved estimate of both the natural frequencies and the mode shapes and also includes damping. The basic of the method follows below.

In order to identify the SDOF autospectral density function at a peak, the mode estimate $\hat{\mathbf{\Phi}}$ is compared with the singular vectors $\mathbf{u}_{\mathrm{ij}}$ for the frequencies around the mode. In this way a SDOF autospectral bell function can be found from which the damped eigenfrequency ω_{d} and the damping ratio ζ can be estimated, see Fig. 3–4. On both sides of the peak a MAC vector between the mode estimate $\hat{\mathbf{\Phi}}$ and the singular vector at a given frequency near the peak is calculated. As long as the MAC value is above a specified MAC rejection level, the corresponding singular value belongs to the SDOF autospectral bell. It is important to notice that the lower the MAC rejection level is, the larger the number of singular values included in the identification of the SDOF autospectral bell function will be. However, this also means that a larger deviation from the mode estimate $\hat{\mathbf{\Phi}}$ is allowed. For that reason an often used MAC rejection level is 0.8. The MAC reads

$$\mathrm{MAC}\left(\hat{\mathbf{\Phi}}, \mathbf{\Phi}_{\mathrm{i}}\right) = \frac{\left(\hat{\mathbf{\Phi}}^{\mathrm{H}}\mathbf{\Phi}_{\mathrm{i}}\right)^{2}}{\left(\hat{\mathbf{\Phi}}^{\mathrm{H}}\hat{\mathbf{\Phi}}\right)\left(\mathbf{\Phi}_{\mathrm{i}}^{\mathrm{H}}\mathbf{\Phi}_{\mathrm{i}}\right)} \tag{3–13}$$

To improve the estimated mode shape $\hat{\mathbf{\Phi}}$, the singular vectors that correspond to the singular values in the SDOF spectral bell function are averaged together. The average is weighted by multiplying the singular vectors with their corresponding singular value, *i.e.* singular vectors close to the peak of the SDOF spectral bell have a large influence on the mode shape estimate. The improved mode shape estimation from a weighted sum $\mathbf{\Phi}_{\mathrm{weight}}$ reads

$$\mathbf{\Phi}_{\mathrm{weight}} = \sum_{i=1}^{n} \mathbf{\Phi}_{\mathrm{i}} s_{\mathrm{i}}, \tag{3–14}$$

where n denotes the number of singular values in the SDOF spectral bell function. From the SDOF autospectral bell function, the damped eigenfrequency ω_{d} and the damping ratio ζ are obtained by transforming the spectral density function to time domain by inverse FFT. A SDOF autocorrelation function is then found and by identification of the positive and negative extremes of this function, the logarithmic decrement δ is estimated according to Eq. (2–33). The damping ratio ζ is then found by Eq. (2–32). Due to broad-banded noise and non-linearities the beginning and the end of the curve may not be straight and for that reason these parts should not be included in the regression. The damped eigenfrequency ω_{d} is found in a similar manner. By a linear regression on the time crossings of the autocorrelation function, the damped eigenfrequency ω_{d} is estimated as the slope of the line. In Fig. 3–5a an illustration of the normalized correlation function for the mode specified in Fig. 3–4 is shown. In addition, the corresponding estimating of the damped eigenfrequency ω_{d} and the logarithmic decrement δ are shown in Fig. 3–5b and Fig. 3–5c, respectively.

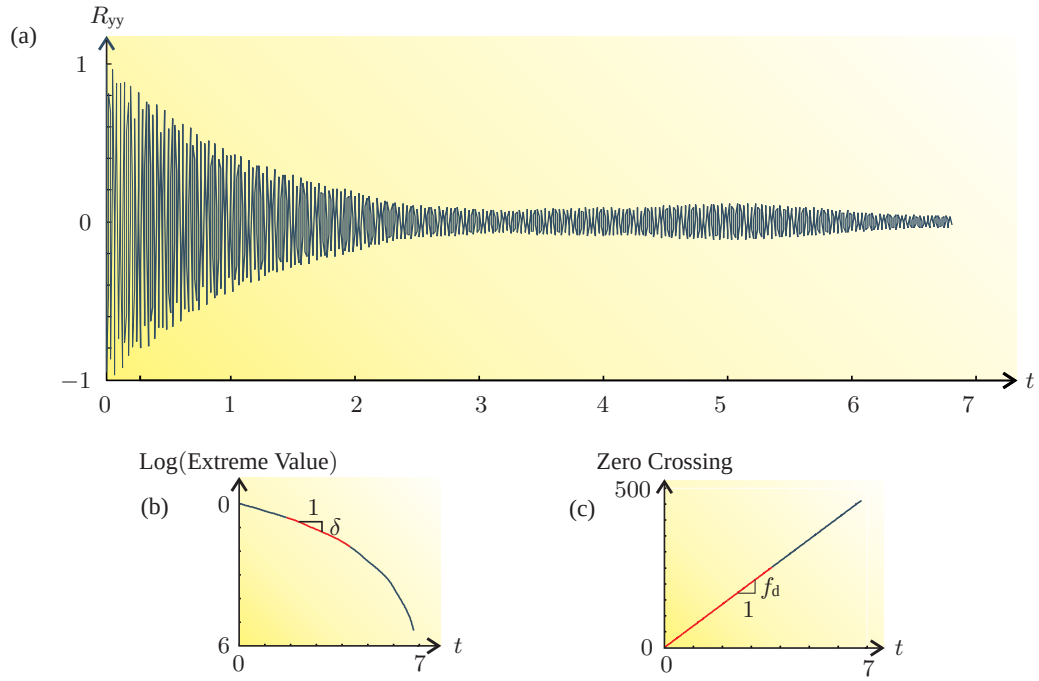

Figure 3–5 Estimation of dynamic properties: (a) Normalized correlation function obtained by inverse FFT, (b) Linear regression on correlation extremes for estimating of damping, (c) Linear regression on correlation crossing times for estimating of frequency.

3.3 Literature Review of Experimental Modal Analysis of Civil Engineering Structures

The modal representation of a structure can be determined analytical. However, in cases where the structural system can not be represented by a lumped mass-spring system, a numerical approximation is made by discretising the structure in a finite number of physical coordinates. A drawback of this approach is the increasing model size required to properly describe complex structures with appropriate detail. A high number of degrees of freedom are needed, which leads to higher calculation time and unchanged inherent modelling accuracy limitations related to non-homogeneous elements, complex materials, boundary conditions etc. Experimental modal analysis addresses these limitations and contributes to validation and improvement of the numerical model (Van der Auweraer 2001).

The overall aim in this section is to present the evolution of experimental modal analysis in the civil engineering field with focus on operational modal identification. An overview of work that has been done during the last years within experimental modal analysis and in particular operational modal identification will be given. It will be documented to what extent operational modal identification has been used for offshore wind turbines. Firstly, a short literature review of traditional experimental modal analysis is presented. The advantages and disadvantages of the technology are illustrated which forms an obvious shift to operational modal identification.

3.3.1 Traditional Experimental Modal Analysis

Traditional experimental modal analysis is characterised by forced vibrations, where the input excitation is measured. Determination of resonance frequencies, damping ratios and mode shapes of structures is well established for this technique. In general, the structure to be identified is artificially excited with a forcing function in a specific point and its response to this excitation is measured together with the forcing signal. Fourier transformation of the time signal makes it possible to calculate all the frequency response functions between the response and the forcing signals, *i.e.* the frequency response matrix. This matrix contains all the information to determine the dynamic properties of the structure.

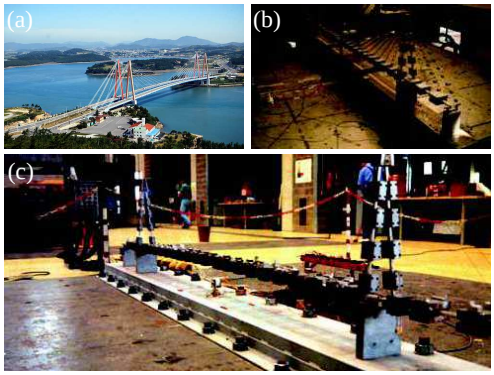

Figure 3–6: Traditional experimental modal test: (a) Jindo Bridge in South Korea, (b) and (c) Shaker table in order to excite the bridge artificial. After Cunha and Caetano (2005).

As already outlined in Section 3.1, excitation of structures can be induced in different ways. Impact excitation has widely been used for smaller civil engineering structures and offers the advantages of quick setup time, mobility and the ability to excite a broad range of frequencies. Askegaard and Mossing (1988), Agardh (1991), Wood *et al.* (1992), Aktan *et al.* (1992), Green and Cebon (1994) and Pate (1997) have all excited full scale bridge structures by impact excitation tools, either by dropping a impact weight or by a bolt gun with impulsive load. However, by use of this method the wave form of the excitation is not controlled. Consequently, a more common method of exciting civil engineering structures is by electrodynamic shakers. Modal tests performed by Shepherd and Charleson (1971), Kuribayashi and Iwasaki (1973), Ohlsson (1986), Cantieni and Pietrzko (1993), Deger *et al.* (1993), Deger *et al.* (1994), Miloslav *et al.* (1994) and Caetano *et al.* (2000) have used shakers to excite bridge structures. An experimental investigation of the Jindo Bridge in South Korea is presented by Caetano *et al.* (2000), where the dynamic properties of the bridge have been identified by using an electrodynamic shaker and a table shaker. Various series of modes shapes were identified at very closely spaced frequencies. Fig. 3–6 shows the physical model of Jindo Bridge. Also for dam structures forced shaker excitation has been used in order to obtain the modal properties, see Duron (1995a) and (1995b), Cantieni (2001) and Nuss *et al.* (2003). Besides, Cantieni *et al.* (1998) have estimated modal parameters of an office building by using shaker excitation. For further information of reviews of forced vibrations in the civil engineering field, see Salawu and Williams (1995), Farrar *et al.* (1999) and Ventura (1997).

Traditional Experimental Modal Analysis of Parked Wind Turbines

For wind turbine structures, the presence of rotational loads and considerable aeroelastic effects makes it difficult to use traditional experimental modal analysis techniques. By use of this method the experimentally determined vibrations are not the pure modes of the turbine. The shaker excitation simply ignores the ambient loads acting on the turbine during operation. However, some few attempts to excite parked wind turbines by measurable excitation forces have been done, see Carne *et al.* (1988) and Molenaar (2003). The need of heavy special excitation devices, the fact that the dynamic properties of operational wind turbines are difficult to obtain and that

shakers have difficulty of producing lower frequency excitations as mentioned in Section 3.1, makes operational modal identification popular.

3.3.2 Operational Modal Identification

In order to obtain dynamic properties of civil engineering structures by operational modal identification, only the response of the structure has to be measured without artificial excitation. The technique has been successfully used for both large and small bridge structures and buildings where traffic and wind loads are used to extract the modal parameters. Hence, the modal parameters are estimated under operational conditions within true boundary conditions and actual force level. As outlined in Section 3.2, the basic assumption of the method is that the natural excitation force is a stationary random process having a flat frequency spectrum and excites the structure in multiple points. This means that the vibration response of a given structure contains all normal modes. During the last years operational modal analysis has been applied to mechanical and aerospace engineering applications, for instance for rotating machinery, on-road testing and in-flight testing (Batel 2002).

Figure 3–7: Ambient excitation of the cable-stayed Vasco da Gama Bridge in Lisbon. (Cunha *et al.* 2004)

The literature on ambient vibration testing of bridge structures is extensive. Among others, Biggs and Suer (1956), Vincent (1958), Vincent *et al.* (1979), Van Nunen and Persoon (1982), Wilson (1986), Swannell and Miller (1987), Agarwal and Billing (1990), Proulx *et al.* (1992), Gates and Smith (1982), Farrar *et al.* (1994), Felber and Cantieni (1996), Ventura *et al.* (1996), Brownjohn (1997), Asmussen *et al.* (1998), Brincker *et al.* (2000) and Cantieni *et al.* (2008) report ambient vibration tests for bridges where traffic, wind and wave loading have been used to excite the structure. An experimental dynamic study of Vasco da Gama Bridge in Lisbon with a total length of 12 km was studied by Peeters *et al.* (2002), see Fig. 3–7. The study was based on an ambient test and a free vibration test in 1998 described by Cunha *et al.* (2001). The intention was to assess the aerodynamic and seismic behaviour of the bridge. The ambient test revealed which modes of the bridge could be excited by natural wind excitation. The aim of the free vibration test was to verify the ambient test results. By use of the Stochastic Subspace Identification method, the modal parameters obtained from the ambient data was compared with those from the free vibration data. Overall, comparable results were obtained. A small deviation was found between the damping ratios. According to Peeters *et al.* (2002) this deviation was caused by that the damping ratio varies with the magnitude of vibrations and that an aerodynamic component was presented in the ambient vibration test due to the relatively high wind speed during the test. Also Cunha *et al.* (2004) has analysed the ambient data of the Vasco da Gama Bridge with the purpose of testing efficiency and accuracy of the Frequency Domain Decomposition and the Stochastic Subspace Identification methods by use of ARTeMIS Extractor. The applications of the two methods led to very close estimates of the modal frequencies and mode shapes. Ambient vibration measurements of large buildings have among others been described by Cheryl and Ventura (1998), Lord and Ventura (2002), Turek *et al.* (2006) and Kuroiwa and Lemura (2000). Based on the study

made by Cheryl and Ventura (1998), the response data of the Heritage Court Building structure was analysed by Brincker and Andersen (2000) using two different techniques, the Frequency Domain Decomposition technique and the Stochastic Subspace Identification technique. Eleven modes were well estimated from the two techniques, where three of them were closely spaced modes around 1.1-1.4 Hz. Overall, comparable modal parameters were obtained from the two methods. As mentioned in Section 3.1, experimental modal analysis can be used to update a finite element model of the structure. Based on the measured response of the 48-story reinforced concrete building One Wal1 Centre in Vancouver from Lord and Ventura (2002), the modal properties of the structure was found by Lord *et al.* (2004). By varying certain parameters in the finite element model of the building, the correlation between the modal properties of the experimental and analytical models almost approximated one.

Operational Modal Identification on Operating Wind Turbines

Full scale measurements on offshore support structures within the oil and gas sector have been practiced for many years, see for instance Cook and Vandiver (1982), John (1983) and Jensen (1990). Literature within experimental analysis of wind turbines is, however, more limited. In general, wind turbines have very specific characteristics and challenging operation conditions, which makes special demands on operational modal identification. In case of a parked wind turbine, the assumptions within operational modal identification are valid, also the ones regarding modal analysis (linear system, stationary and time invariant), except that aeroelastic effects are considerable even in case of a parked wind turbine, see Liingaard (2006) as an example of using operational modal identification for a parked wind turbine. In addition, Osgood *et al.* (2010) have compared the modal properties of a parked wind turbine excited by a shaker with an operational modal analysis based on Stochastic Subspace Identification, where the same structure is subjected to wind excitation. The aim of the study was to verify operational modal identification for parked wind turbines. The two ways of estimating modes agreed very well, which clearly shows the advantage of operational modal identification. According to Tcherniak *et al.* (2010), two numbers of inherent problems reveal when using operational modal identification on operational wind turbines:

1. The assumption of structure time invariance is violated. The nacelle rotates about the tower, the rotor rotates around its axis and the pitch of the blades may changes. A complication is that the modal frequencies are dependent on the turbine rotation speed.

2. In the operational modal identification theory it is assumed that the excitation forces must have broadband frequency spectra, they must be distributed over the entire structure and they must be uncorrelated. Forces due to wind turbulence fulfill these requirements. However, the effect of rotor rotation changes the nature of aerodynamic forces. The shape of the input spectra transforms from being flat to a curve with distinct peaks at the rotation frequencies and its harmonics. Moreover, the excitation forces now become correlated around the rotation frequency and its harmonics.

As indicated, application of operational modal analysis to operational wind turbines is not a straight forward task. As the input forces are not measured in operational modal identification, it is important to identify and separate the harmonic components (deterministic signals) from the structural modes and eliminate the influence of the harmonic components in the modal estimation

process. According to Jacobsen *et al.* (2007), the harmonic components cannot be removed by simple filtering as this would significantly change the poles of the structural modes and thereby their natural frequency and modal damping. Actually, harmonic components can easily be seen when plotting the singular values from the FDD technique. The rank of the matrix containing the singular values is 1 at frequencies where only one mode is dominating, see Fig. 3–4. For harmonic components a high rank will be seen at these frequencies, as all modes will be excited Jacobsen (2005). An elegant way of identifying and removing harmonics components is by Kurtosis techniques. Basically, the idea is that the probability density function (PDF) for structural modes excited by stochastic excitation from wind and waves differ significantly from the PDF for deterministic excitation such as harmonic components. Therefore, testing of the shape of the PDF of the measured response is a way of determining, whether sinusoidal excitation forces are present by use of Kurtosis techniques. The identified harmonics are removed by performing a linear interpolation across the harmonic components in the SDOF function (Gade *et al.* 2009). The method is implemented in ARTeMIS Extractor in the Enhanced Frequency Domain Decomposition (EFDD) technique.

Jacobsen *et al.* (2007) demonstrated the harmonic detection approach on measurements from an aluminum plate structure excited by a combination of a single sinusoidal signal and a broadband stochastic signal. By comparing the modal parameters obtained with pure stochastic excitation of the same structure, the approach showed good agreement, even in the case of having a harmonic component located at the peak of a structural mode sensible modal estimates were found. Also Gade (2009) and Andersen *et al.* (2008) have demonstrated the harmonic detection approach with success on measurements from a gearbox and a gravity dam structure, respectively.

Estimations of natural frequencies and damping ratios of an onshore wind turbine for different mean wind speeds have been studied by Hansen *et al.* (2006). An excitation method, where turbine vibrations were obtained by blade pitch and generator torque variations, was compared with the operational modal analysis algorithm Stochastic Subspace Identification. For the excitation method the decaying response after the end of excitation gave an estimate of the damping. However, the conclusion of the excitation method was that the excited turbine vibrations were not pure modal vibrations and hence, the estimated modal properties were not the actual modal properties of the wind turbine. For the operational modal identification analysis three months of measurements were scanned to find 1-3h long periods of low standard deviations for wind and rotor speeds in order to improve the assumption of a time invariant system. For that reason several 10 min measurements series were collected. From the Stochastic Subspace Identification it was found that the natural frequency of the first two tower bending modes was almost constant with the mean wind speed (Campbell diagram) whereas the damping of the lateral tower mode decreased from 50% logarithmic decrement at the rated wind speed to about 20% at higher wind speeds.

Tcherniak *et al.* (2010) also presented the application of operational modal identification by use of Stochastic Subspace Identification of simulated response of a wind turbine structure by use of a commercial aeroelastic code. The authors discussed the time invariants of the system due to the rotating rotor. This causes time dependent eigenvalues and eigenmodes which do not have a meaning as modal frequencies, modal damping and mode shapes. In order to avoid the time dependent modal parameters and thereby a time dependent equation of motion, the authors made use of Coleman transformation. Basically, the technique converts the motion of each individual blade described in the rotating blade frame into the ground-fixed frame. More information of this

technique, see Tcherniak *et al.* (2010) and Bir (2008). In addition, Ozbek and Rixen (2011) have used operational modal identification to estimate the modal properties of a parked and operational 2.5 MW wind turbine. By use of the well-known output-only modal method Natural Excitation Technique (NEXT), the estimation of the modal properties was done. The authors concluded that a suitable selection of low noise ratio data series, a sufficient data length and a check of the changes at excitation levels, were needed in order to obtain realistic modal parameters. See Carne and James (2010) for more information about the NEXT algorithm.

3.4 Summary

In this chapter the concepts of experimental modal analysis have been presented. Focus has been on explaining the difference between traditional experimental modal analysis and operational modal identification. A large number of operational modal analysis algorithms exist. However, this chapter has only presented the theory of the so-called Frequency Domain Decomposition technique. A literature review of experimental modal analysis shows that the traditional experimental modal analysis and operational modal identification widely have been used for many different civil engineering structures such as large cable-stayed bridges, tall buildings and dam structures. However, due to the complex dynamic behaviour of an operational wind turbine careful application of operational modal identification must be considered for this type of structure. During operation, wind turbines are subject to dynamic loads, because the aerodynamic and gravitational loads vary with time as the turbine rotates. It must be ensured that the operational condition of the wind turbine preclude resonance frequencies and thereby minimizing dynamic loads and lengthening the service life of the structure. Some of the main conclusions in this chapter are:

Modal updating is a method to refine and validate computer simulations in order to develop accurate structural models by use of extensive experimental testing.

Traditional experimental modal analysis or input-output modal analysis is performed by measuring the input and output responses for a linear, time-invariant system. A set of frequency response functions relate the applied force and corresponding response at several pairs of points along the structure. The modal parameters (natural frequencies, modal damping ratios and mode shapes) are found by fitting a model to the frequency response functions.

Impact excitation is a method to excite structures artificially. Impulse hammers are typically used for smaller structures, whereas large structures like bridges are excited by dropping weights onto a shock absorber that prevent rebound.

Electrodynamic excitation is like impact excitation a method to excite structures artificially. The shakers offer the advantage of being able to vary the input waveform.

Operational modal identification is applied to extract the modal parameters based on measuring only the response of a structure under ambient or operational excitation. The method rely on the assumption, that the input forces are derived from Gaussian white noise and excite in multiple points. The great advantage of operational modal identification is in providing the dynamic model of the structure under actual operating conditions and real boundary conditions.

Frequency Domain Decomposition technique is an algorithm used in operational model identification. By introducing a decomposition of the spectral density function matrix, the response can be separated into a set of single degree of freedom systems, each corresponding to an individual mode.

Overall, this memorandum has given an introduction to experimental modal analysis, where advantages and disadvantages of methodologies within the experimental field have been presented. The intention has been to document to what extent operational modal identification can be used for wind turbine structures. The memorandum documents that special care must be considered when using operational modal identification on wind turbine structures. Different factors affect the identified system parameters, which are briefly given below:

1. Ensuring a reliable and accurate measurement of the responses is crucial to extract the dynamic properties of a structure. High noise to signal ratio limits the accuracy of the measurements.

2. The time varying nature of wind turbine structures must be considered. A way to handle this problem is by finding a suitable period, where blade pitch angle, wind speed and rotor speed remain unchanged. Alternatively, the Coleman transformation can be used to get rid of time-dependencies in the equation of motion and obtain meaningful modal parameters.

3. The major assumption in operational modal identification is steady state broadband random excitation. Wind excitation fulfills this requirement but the resulting excitation from the aerodynamic forces will contain significant components on the 1P, 3P and 6P harmonics from the rotating rotor. These harmonics must be identified and separated from the structural modes. Kurtosis techniques followed by linear (EFDD) interpolations before estimation of modal parameters will handle this problem.

References

Agardh, L. (1991). Modal Analysis of Two Concrete Bridges in Sweden. In *Structural Engineering International*, Volume 1, Sweden, pp. 34–39.

Agarwal, A.C. and Billing, J.R. (1990). Dynamic Testing of the St. Vincent Street Bridge. In *Proceedings of the Annual Conference, Canadian Society for Civil Engineering*, Volume 4, pp. 163–181.

Aktan, A.E., Zwick, J., Miller, R.A., and Sharooz, B.M. (1992). Nondestructive and Destructive Testing of a Decommissioned RC Slab Highway Bridge and Associated Analytical Studies. *Transportation Research Record*.

Andersen, P. (1997). *Identification of Civil Engineering Structures using Vector ARMA Models*. PhD thesis, Aalborg University, Denmark.

Andersen, P. (2011). ARTeMIS User Training Course. Technical Course, Structural Vibration Solution.

Andersen, P., Brincker, R., Ventura, C., and Cantieni, R. (2008). Mode Estimation of Civil Structures Subject to Ambient and Harmonic Excitation. In *Proceedings of the 26th International Modal Analysis Conference (IMAC)*, Orlando, Florida.

API (2000). Recommended practice for planning, designing and constructing fixed offshore platforms, *Rp2a-wsd*. American Petroleum Institute, Dallas, Texas, USA.

Askegaard, V. and Mossing, P. (1988). Long Term Observation of RC-bridge Using Changes in Natural Frequencies. *Nordic Concrete Research* **7**, 20–27.

Asmussen, J.C., Brincker, R., and Rytter, A. (1998). Ambient Modal Testing of the Vestvej Bridge Using Random Decrement. In *Proceedings of the 16th International Modal Analysis Conference (IMAC)*, Santa Barbara, California, pp. 922–928.

Batel, M (2002). Operational Modal Analysis - Another Way of Doing Modal Testing. *Journal of Sound and Vibration*, 22–27.

Bendat, J.S. and Piersol, A.G. (1980). *Engineering Applications of Correlation and Spectral Analysis* (2 ed.). New York: John Wiley & Sons, Inc.

Bendat, J.S. and Piersol, A.G. (2000). *Random Data: Analysis and Measurement Procedures* (3 ed.). New York: John Wiley & Sons, Inc.

Biggs, J.M.. and Suer, H.S. (1956). Vibration Measurements on Simple-Span Bridges. Highway Research Board Bulletin 1–15, Washington D.C.

Bir, G. (2008). Multiblade Coordinate Transformation an Its Application to Wind Turbine Analysis. In *Proceedings of ASME Wind Energy Symposium*, Reno, Nevada.

Brincker, R. and Andersen, P. (2000). Ambient Response Analysis of the Heritage Court Building Structure. In *Proceedings of the World Forum on Smart Materials and Smart Structures Technology*, Chogqing & Nanjing, China.

Brincker, R., Andersen, P., and Frandsen, J.B. (2000). Ambient Response Analysis of the Great Belt Bridge. In *Proceedings of the 18th International Modal Analysis Conference (IMAC)*, San Antonio, Texas.

Brincker, R., Andersen, P., and Zang, L. (2000). Modal Identification from a Ambient Reponse using Frequency Domain Decomposition. In *Proceedings of the 18th International Modal Analysis Conference (IMAC)*, pp. 625–630.

Brincker, R., Ventura, C.E., and Andersen, P. (2001). Damping Estimation by Frequency Domain Decomposition. In *Proceedings of the 19th International Modal Analysis Conference (IMAC)*, Kissimmee, Florida, pp. 698–703.

Brownjohn, J.M (1997). Vibration Characteristics of a Suspension Footbridge. *Journal of Sound and Vibration* **202**, 29–46.

Caetano, E., Cunha, A., and Taylor, C.A. (2000). Investigation of Dynamic Cable-Deck Interaction in a Physical Model of a Cable-Stayed Bridge Part I: Modal Analysis. *International Journal Earthquake Engineering and Structural Dynamics* **29**, 481–498.

Cantieni, R. (2001). Assessing a Dam's Structural Properties Using Forced Vibration Testing. In *Proceedings of IABSE International Conference on Safety, Risk and Reliability - Trends in Engineering*, Malta.

Cantieni, R., Brehm, M., Zabel, T., V. Rauert, and Hoffmeister, B. (2008). Ambient Testing and Model Updating of a Bridge for High-Speed Trains. In *Proceedings of the 26th International Modal Analysis Conference (IMAC-XXVI)*, Orlando, Florida.

Cantieni, R. and Pietrzko, S. (1993). Modal Testing of a Wooden Footbridge Using Random Excitation. In *Proceedings of the 11th International Modal Analysis Conference*, Volume 2, pp. 1230–1236.

Cantieni, S.J., Pietrzko, S., , and Deger, Y. (1998). Modal Investigation of an Office Building Floor. In *Proceedings of the 16th International Modal Analysis Conference*, Volume 2, pp. 1172–1178.

Carne, T.G. and James, G.H. (2010). The Inception of OMA in the Development of Modal Testing Technology for Wind Turbines. *Mechanical Systems and Signal Processing* **24**, 1213–1226.

Carne, T.G., Lauffer, J.P., and Gomez, A.J. (1988). Modal Testing of a Very Flexible 110 m Wind Turbine Structure. In *Proceedings of 6th Internationale Modal Analysis Conference*, Kissimmee, Florida.

Cheryl, D. and Ventura, C.E. (1998). Ambient Vibration Measurements of Heritage Court Tower. Earthquake Engineering Research, University of British Columbia.

Cook, M.F. and Vandiver, J.K. (1982). Measured and Predicted Dynamic Response of a Single Pile Platform to Random Wave Excitation. In *Proceedings of the 14th OTC*, Houston, Texas, pp. 637–642.

Cunha, A. and Caetano, E. (2005). Experimental Modal Analysis of Civil Engineering Structures. In *Intertional Modal Analysis Conference IOMAC*, Copenhagen, Denmark, pp. 12–20.

Cunha, A., Caetano, E., Brincker, R., and Andersen, P. (2004). Identification from the Natural Response of the Vasco Da Gama Bridge. In *Proceedings of the 22nd International Modal Analysis Conference IMAC*, Detroit, Michigan.

Cunha, A., Caetano, E., and Delgado, R. (2001). Dynamic Tests on Large Cable-Stayed Bridge: An Efficient Approach. *Journal of Bridge Engineering* **6**, 54–62.

Damkilde, L. (1998). Introduktion til Dynamik. Technical Report, Aalborg University.

Danish Wind Industry Association (2011). http://www.windpower.org/en/.

Deger, Y., Cantieni, R., and Pietrzko, S. (1994). Modal Analysis of an Arch Bridge: Experiment, Finite Element Analysis and Link. In *Proceedings of the 12th International Modal Analysis Conference*, Volume 1, pp. 425–432.

Deger, Y., Cantieni, S.J., Pietrzko, S., Rücker, W., and Rohrmann, R. (1993). Modal Analysis of a Highway Bridge: Experiment, Finite Element Analysis and Link. In *Proceedings of the 13th International Modal Analysis Conference*, Volume 2, pp. 1141–1149.

DNV (2001). Foundations, *Classification Notes No. 30.4*. Det Norske Veritas Classifications A/S, Høvik, Norway.

DNV (2010). Recommended Practice DNV-RP-C205 - Environmental Conditions and Environmental Loads. Det Norske Veritas Classifications A/S, Høvik, Norway.

Duron, Z.H (1995a). Seven Mile Vibration Testing Results from the First Series of Test Performed February 20-07. Research Report Prepared for B.C Hydro and Power Authority, Canada.

Duron, Z.H (1995b). Seven Mile Vibration Testing Results from the Second Series of Test Performed August 14-20. Research Report Prepared for B.C Hydro and Power Authority, Canada.

Ewins, D.J. (2000). *Modal Testing: Theory, Practice and Application* (2 ed.). England: Research Studies Press LDT.

Farrar, C.R., Baker, W.E., Bell, T.M., Cone, K.M., Darling, T.W., Duffey, T.A., Eklund, A., and Migliori, A. (1994). Dynamic Characterization and Damage Detection in the I-40 Bridge over the Rio Grande. Technical Report 153, United States.

Farrar, C.R., Duffey, T.A., Cornwell, P.J., and Doebling, S.W. (1999). Excitation Methods for Bridge Structures. In *17th International Modal Analysis Conference*, Florida, USA.

Felber, A.J. and Cantieni, R. (1996). Introduction of a New Ambient Vibration System - Description of the System and Seven Bridge Tests. Technical Report, Duebendorf.

Gade, S., Møller, N.B., Herlufsen, H., and Kostantin-Hansen, H. (2005). Frequency Domain Techniques for Operational Modal Analysis. In *Proceedings of the 1st IOMAC Conference*.

Gade, S., Schlombs, R., Hundeck, C., and Fenselau, C. (2009). Operational Modal Analysis on a Wind Turbine Gearbox. In *IMAC-XXVII: Conference & Exposition on Structural Dynamics*.

Gates, J.H.. and Smith, M.J. (1982). Verification of Dynamic Modeling Methods by Prototype Excitation. Technical Report 192, California.

Global Wind Energy Council (2010). Global Wind Report - Annual Market Update 2010. Technical Report.

Green, M.F. and Cebon, D. (1994). Dynamic Response of Highway Bridges to Heavy Vehicle Loads: Theory and Experimental Validation. *Journal of Sound and Vibration* **170**, 51–78.

Hansen, M.H., Thomsen, K., Fuglsang, P., and Knudsen, T. (2006). Two Methods for Estimating Aeroelastic Damping of Operational Wind Turbine Modes from Experiments. *Wind Energy* **9**, 179–191.

Jacobsen, N. (2005). Identifying Harmonic Components in Operational Modal Analysis. In *Twelfth International Congress on Sound and Vibration*, Lisbon, Portugal.

Jacobsen, N.J., Andersen, P., and Brincker, R. (2007). Eliminating the Influence of Harmonic Components in Operational Modal Analysis. In *Proceedings of the 28th Internationale Modal Analysis Conference IMAC XXVIII*, Orlando, Florida.

Jensen, C. (2011). Numerical Simulation of Gyroscopic Effects in Ansys. Masters thesis, Aalborg University, Denmark.

Jensen, J.L (1990). Full-Scale Measurements of Offshore Platforms. Technical Report, Aalborg University.

John, H.D. (1983). The Measurement of Performance of Offshore Piled Foundation - A Review. *Ground Engineering* **2**, 24–30.

Kuribayashi, E. and Iwasaki, T. (1973). Dynamic Properties of Highway Briges. In *Proceedings of the 5th World Conference on Earthquarke Engineering*, pp. 938–941.

Kuroiwa, T. and Lemura, H (2000). Comparison of Modal Identification of Output-Only Systems with Simultaneous and Non Simultaneous Monitoring. In *Proceedings of the 18th International Modal Analysis Conference (IMAC)*, San Antonio, Texas, pp. 1081–1087.

Larsen, J.W. (2005). *Nonlinear Dynamics of Wind Turbine Wings*. PhD thesis, Aalborg University, Denmark.

Leblanc, C. (2009). *Design of Offshore Wind Turbine Support Structures*. PhD thesis, Aalborg University, Denmark.

Liingaard, M. (2006). *Dynamic Behaviour of Suction Caissons*. PhD thesis, Aalborg University, Denmark.

Liu, Z. and Frigaard, P. (2001). Generation and Analysis of Random Waves. Technical Report, Aalborg University.

Lord, J-F. and Ventura, C.E. (2002). Measured and Calculated Modal Characteristics of a 48-Story Tunded Mass System Building in Vancouver. In *International Modal Analysis Conference-XX: A Conference on Structural Dynamics Society for Experimental Mechanics*, Volume 2, Los Angeles, USA, pp. 1210–1215.

Lord, J-F., Ventura, C.E., and Dascotte, E. (2004). Automated Model Updating Using Ambient Vibration Data form a 48-Storey Building in Vancouver. In *Proceedings of the 22th Internationale Modal Analysis Conference IMAC*, Detroit, MI.

Miloslav, B., Vladimir, B., and Michal, P. (1994). Dynamic Behaviour of Footbridge by Analysis and Test. In *Proceedings of the 13th International Modal Analysis Conference*, Volume 1, pp. 687–693.

Molenaar, D.P. (2003). Experimental Modal Analysis of a 750 kW Wind Turbine for Structural Modal Validation. In *41st Aerospace Sciences Meeting and Exhibit*, Reno, Nevada.

Nielsen, S.R.K (2004). *Linear Vibration Theory* (1 ed.). Denmark: Aalborg Tekniske Universitetesforlag.

Nuss, L.K., Chopra, A.K., and Hall, J.F. (2003). Comparison of Vibration Generator Tests to Analyses Including Dam-Foundation-Reservoir Interaction for Morrow Point Dam. In *The Commission Internationale Des Grande Barrages, 20th Congress of Large Dams*.

Ohlsson, S. (1986). Modal Testing of the Tjorn Bridge. In *Proceedings of the 4th International Modal Analysis Conference*, Florida, pp. 599–605.

Osgood, R., Bir, G., and Mutha, H. (2010). Full-Scale Modal Wind Turbine Tests: Comparing Shaker Excitation with Wind Excitation. In *Proceedings of the 28th Internationale Modal Analysis Conference IMAC XXVIII*, Jacksonville, Florida, pp. 113–124.

Ozbek, M. and Rixen, D.J. (2011). Optical Measurements and Operational Modal Analysis on a Large Wind Turbine: Lessons Learned. In *Conference Proceedings of the Society for Experimental Mechanics Series*, pp. 257–276.

Pate, J.W. (1997). Dynamic Testing of a Highway Bridge. In *Proceedings of the 15th Internationale Modal Analysis Conference*, pp. 2028–2037.

Peeters, B., De Roeck, G., Caetano, E., and Cunha, A. (2002). Dynamic Study of the Vasco da Gama Bridge. In *Proceedings of the International Conference on Noise and Vibration Engineering ISMA*, Volume 2, pp. 545–554.

Proulx, J., Herbert, D., and Paultre, P. (1992). Evaluation of the Dynamic Properties of a Steel Arch Bridge. In *Proceedings of the 10th International Modal Analysis Conference*, Volume 2, San Diego, pp. 1025–1031.

Salawu, O.S. and Williams, C. (1995). Review of Full-Scale Dynamic Testing of bridge structures. *Engineering Structures* **17**, 113–121.

Shepherd, R. and Charleson, A.W. (1971). Experimental Determination of the Dynamic Properties of a Bridge Substructure. *Bulletin of the Seismological Society of America* **61**, 1529–1548.

Smith, S.W. (1997). *The Scientist and Engineer's Guide to Digital Signal Processing* (1 ed.). USA: California Technical Publishing.

Swannell, P. and Miller, C.W. (1987). Theoretical and Experimental Studies of a Bridge Vehicle System. *Proceedings of the Institute of Civil Engineers, Part 2* **83**, 613–615.

Tcherniak, D., Chauhan, S., Rosseth, M., Font, I., Basurko, J., and Salgado, O. (2010). Output-Only Modal Analysis on Operating Wind Turbines: Application to Simulated Data. In *European Wind Energy Conference*, Warsaw, Poland.

Tcherniak, T., Chauhan, S., and Hansen, M.H. (2010). Applicability Limits of Operational Modal Analysis to Operational Wind Turbines. In *Proceedings of the 28th Internationale Modal Analysis Conference IMAC XXVIII*, Volume 1, Jacksonville, Florida, pp. 317–327.

Turek, M., Thibert, C., K. Ventura, and Kuan, S. (2006). Ambient Vibration Testing of Three Unreinforced Brick Masonry Buildings in Vancouver, Canada. In *Proceedings of the 24th International Modal Analysis Conference (IMAC)*, St. Louis, Missouri.

Van der Auweraer, H. (2001). Structural Dynamic Modeling using Modal Analysis: Applications, Trends and Challenges. In *IEEE Instrumentation and Measurement*, Budapest, Hungary, pp. 1502–1509.

Van Nunen, J.W.G. and Persoon, A.J. (1982). Investigation of the Vibrational Behavior of a Cable-Stayed Bridge Under Wind Loads. *Engineering Structures* **4**, 99–105.

Ventura, C.E., Felber, A.J., and Stiemer, S.F. (1996). Determination of the Dynamic Characteristics of the Colquiz River Bridge by Full-Scale Testing. *Canadian Journal of Civil Engineering* **23**, 536–548.

Ventura, C.E. and Horyna, T. (1997). Structural Assessment by Modal Analysis in Western Canada. In *Proceedings of the 15th Internationale Modal Analysis Conference*, pp. 101–105.

Vestas (2011). Vestas V90-1.8/2.0 MW. Technical Report.

Vincent, G.S. (1958). Golden Gate Bridge Vibration Study. *Journal of the Structural Division ASCE* **84**.

Vincent, P.G., Hooley, R., Morgenstern, B.D., Rainer, J.H., and van Selst, A.M. (1979). Suspension Bridge Vibrations: Computed and Measured. *Journal of the Structural Division ASCE* **105**, 859–874.

Wilson, J.C (1986). Analysis of the Observed Seismic Response of a Highway Bridge. *Earthquake Engineering and Structural Dynamics* **14**, 339–354.

Wood, M.G., Friswell, M.I., and J.E.T., Penny (1992). Exciting Large Structures using a Bolt Gun. In *Proceedings of the 10th International Modal Analysis Conference*, pp. 233–238.

Zang, R., L. Brincker and Andersen, P. (2001). Modal Indicators for Operational Modal Identification. In *Proceedings of the 19th International Modal Analysis Conference (IMAC)*, Kissimmee, Florida, pp. 746–752.

ISSN 1901-7278
DCE Lecture Notes No. 13